University of Tartu

Faculty of Science and Technology

Institute of Chemistry

Karl Karu

COMPUTATIONAL INVESTIGATION OF IONIC LIQUIDS

MSc thesis (30 EAP)
Chemistry

Supervisors:

PhD Vladislav Ivaništšev
MSc Meeri Lembinen

Tartu 2017

Resümee/Abstract

Ioonsete vedelike uurimine arvutuskeemia meetoditega

Ioonseid vedelikke on viimaste aastakümnete jooksul laialdaselt uuritud, et kasutada ära nende unikaalseid ja varieeritavaid füsikokeemilisi omadusi. Kuna ioonsete vedelike hind on kõrge ja võimalikke ioonide kombinatsioone on väga palju, siis on nad ahvatlevaks objektiks arvutuskeemiale. Samas on ioonsete vedelike simuleerimine keerukas, sest ioonses vedelikes esineb palju erinevaid interaktsioone, mida rakendatav metoodika peab suutma adekvaatselt kirjeldada. Antud töös võrdlesime tihedusfunktionaali teooria meetodite PBE, M06-L, SCAN, SCAN0 ning B2PLYP võimet kirjeldada ioonseid vedelikke. Referentsmeetodina kasutati DLPNO-CCSD(T) meetodit, mis ekstrapoleeriti täieliku baasfunktsioonide komplektini. Käesolevas töös on lisaks koostatud tihedusfunktionaali teoorial põhinev mudel ioonsete vedelike stabiilsuse ja viskoossuse hindamiseks. Antud robustne kuid efektiivne mudel võimaldab korreleerida kvantkeemia arvutustulemusi makroskoopiliste omadustega.

CERCS: P410 Teoreetiline ja kvantkeemia; P400 Füüsikaline keemia; P401 Elektrokeemia

Märksõnad: ioonsed vedelikud, kvantkeemia, arvutuskeemia, tihedusfunktsionaali teooria, suuremahuline uurimine, elektrokeemiline stabiilsus, viskoossus

Computational investigation of ionic liquids

Ionic liquids have been extensively studied over the past few decades to take advantage of their fine-tunable physicochemical properties. Due to the high cost of synthesis as well as a large number of ion combinations, it is beneficial to investigate them using computational chemistry methods. At the same time, it is also challenging to find a suitable computational approach that captures the whole variety of different types of interactions present in ionic liquids. In this work, we have compared the performance of PBE, M06-L, SCAN, SCAN0, and B2PLYP density functionals when describing ionic liquids. DLPNO-CCSD(T) method extrapolated to the complete basis set limit is used as a reference. In addition, we have constructed a density functional theory-based model to evaluate the electrochemical stability and viscosity of ionic liquids. This simple yet efficient model correlates the macroscopic properties to our computational results.

CERCS: P410 Theoretical chemistry, quantum chemistry; P400 Physical chemistry; P401 Electrochemistry

Keywords: ionic liquids, quantum chemistry, computational chemistry, density functional theory, high-throughput computation, electrochemical stability, viscosity

Table of contents

List of figures

List of tables

Abbreviations, constants, definitions

CCSD(T) – The coupled cluster method with single and double excitations with perturbative triple excitations

DLPNO-CCSD(T) – The domain-based local pair natural orbital CCSD(T) method

DFT – Density functional theory

PBE – Exchange–correlation functional by Perdew–Burke–Ernzerhof

M06-L – The local Minnesota 06 exchange–correlation functional

B2PLYP – The double-hybrid exchange–correlation functional, which combines the exchange energies from Becke 1988 functional and Hartree–Fock method, with the correlation energies from Lee–Yang–Parr functional and second-order perturbation theory

SCAN – The strongly constrained and appropriately normed density exchange–correlation functional by Sun *et al.*

SCAN0 – Hybrid version of SCAN, which combines Hartree–Fock exchange with that of SCAN by Hui and Chai

D3 – Grimme's dispersion correction

BSSE – Basis set superposition error

CP – Counterpoise scheme for evaluating BSSE

GGA – Gradient-generalized approximation

$\boldsymbol{E}_{\mathbf{int}}$ – Interaction energy of an ionic pair

$\Delta\boldsymbol{H}_{\mathbf{vap}}$ – Heat of vaporization

$\boldsymbol{D}$ – Self-diffusion coefficient

MAXD – Maximum deviation

MAD – Mean absolute deviation

MD – Mean deviation

SDEP – Standard error of prediction

LUMO – Lowest unoccupied molecular orbital

HOMO – Highest occupied molecular orbital

ΔSCF – Delta self-consistent field method

IE – Ionization energy

EA – Electron affinity

$\boldsymbol{e}$ – Elementary charge ($1.60 \cdot 10^{-19}$ C)

EW – Electrochemical (stability) window

$\boldsymbol{E}_{\mathbf{a}}$ – Activation energy

$\boldsymbol{E}_{\mathbf{disp}}$ – Energy of the dispersion interaction in an ionic pair determined by D3 method

$\boldsymbol{V}_{\mathrm{m}}$ – Molar volume

$\boldsymbol{M}$ – Madelung constant

1 Introduction

The so-called room-temperature ionic liquids (salts with melting points below 100–150°C) have been extensively studied over the past few decades to take advantage of their fine-tunable physicochemical properties. Ionic liquids possess many advantages over the traditional aqueous and organic solutions such as higher electrochemical and thermal stability, negligible vapor pressure and high charge density [1, 2].

However, high cost inhibits the investigation and the widespread commercial utilization of room-temperature ionic liquids, especially when a reasonable degree of purity is required [3]. Thus, it is beneficial to incorporate computational chemistry methods into the design of novel ionic liquids, which allows evaluating the desired properties before synthesis [4]. High-throughput computational screening of ionic liquids as well as other components of the energy storage systems have been succesfully conducted before [5–9].

1.1 Problem overview

Accurate simulations of condensed matter, especially of soft matter such as ionic liquids, demand large amounts of computational power to describe its mesoscopic structure [10,11]. The quantum chemistry "gold standard" – the coupled cluster method with single and double excitations with perturbative triple excitations (CCSD(T)) – is not applicable to such systems. As the CCSD(T) speed scales as the 7th order of the number of employed basis functions, it is commonly applied to single molecules, while soft matter models usually consist of dozens of molecules [12, 13].

In calculations of ionic liquids, density functional theory (DFT) methods offer a good trade-off between accuracy and cost [10, 14, 15]. In DFT the electronic density is considered instead of wavefunctions and calculations scale as the 3rd order of employed basis functions. For this reason, the DFT methods are widely employed in chemistry [16, 17]. They can tackle condensed systems and can even be used for DFT-based molecular dynamics (MD) simulations. However, there are many flavors of DFT within a hierarchy of DFT methods that is often referred as Jacob's ladder [18]. Thus, DFT calculations can be carried out with different levels of accuracy and speed depending on the needs of a particular task.

In certain cases, instead of the DFT-based calculations, one could even resort to those methods that employ classical mechanics (*e.g.* molecular mechanics, molecular dynamics, Monte Carlo), thus completely neglecting the electronic structure and simulating larger systems. Of course, electronic effects are not captured implicitly in these methods; therefore they require empirical parametrization and are not guaranteed to yield relevant results for "irregular" systems, . different than the systems used in developing in the method's parametrization [10].

Depending on the task at hand, the employed computational model and method need to be chosen appropriately and pre-tested to fit the required criteria of speed and accuracy. In the case of ionic liquids, the selected method should be accurate enough to describe all of the complex physical interactions between ions and yet be able to characterize small associates such as ionic pairs as well as mesoscopic structures of ionic liquid bulk or even ionic liquid at interfaces. This task is not trivial and requires the utilization of state-of-the-art methods, sophisticated models as well as the combination of different approaches [10, 19, 20].

1.2 Goals

In the current work, we have investigated ionic liquids with DFT methods. As mentioned above, DFT is more cost efficient than CCSD(T). Furthermore, DFT can be corrected to account for some of the known systematic errors to improve its accuracy [21, 22]. On the way to large-scale DFT-based MD simulations for more specific case studies, we have evaluated the performance of several DFT methods against domain-based local pair natural orbital CCSD(T) (DLPNO-CCSD(T)) results for a wide variety of ionic liquids associates.

The first goal of this work was to compare the performance of widely used density functionals PBE, M06-L, and B2PLYP with a novel SCAN density functional [23] on a set of 48 ionic liquid pairs. The SCAN functional was previously shown to yield accurate results for diversely bonded materials [24]. If SCAN performs as well on describing ionic liquids, then it could be a valuable tool for condensed matter simulations and high-throughput ionic liquid design. We have tested the fitness of SCAN for simulations of ionic liquids. In particular, we applied Grimme's dispersion correction (D3) [25], self-interaction error correction (through hybrid SCAN0 functional) [26], and basis set superposition error (BSSE) correction with Counterpoise (CP) scheme [27] to find the best performing combination. These corrections are known to benefit other density functionals [14, 21, 22, 28], so as expected we show that they also improve the results of SCAN.

The second goal of this work was to correlate energies extracted from the quantum chemical computation to physicochemical properties such as electrochemical stability and viscosity, which are both of the utmost importance in practical applications. Since our ionic liquid model composes only of single ionic pairs *in vacuo*, the obtained values can not be compared to experiment directly and require additional fitting. However, the results are still insightful, as they provide the relative ranking of the studied 48 ionic liquids. We suggest that the developed computational model can be employed to design novel ionic liquids with a desirable combination of electrochemical stability and viscosity.

2 Problem review

As stated in the previous chapter, we choose DFT methods to run electronic structure calculations of ionic liquids due to a good trade-off between accuracy and cost [14]. The heart of the DFT methods is the employed exchange–correlation functional. The exact form of which is not known and is not expected to be simpler than the solution of the corresponding Schrödingers equation in wavefunction theory (. analytically unsolvable for systems with more than one electrons) [16].

The exchange–correlation functional, by definition, is meant to include the portion of energy that is not analytically obtainable from electron density. Those problematic energy terms are, as the name suggests, exchange and correlation energy, which can only be found exactly for uniform electronic gas. In short, exchange energy is the energy yielded in a quantum mechanical effect, where two degenerate particles exchange their wavefunctions, and correlation energy is the interaction between particles (*e.g.* Coulombic repulsion between electrons) [29].

There are many different density functionals proposed throughout literature, while there is none that is the most physically sound. Therefore, the choice of the employed density functional is non-trivial and may depend on the task at hand, because they all operate under various approximation.

2.1 DFT methods

In a pure DFT approach, there are no orbitals included whatsoever. Kohn and Sham incorporated non-interacting one-electron orbitals to DFT to estimate the kinetic energy [30]. The resulting method is not entirely accurate for finding kinetic energy, and it neglects the electron–electron interaction completely. More advanced exchange–correlation functionals include terms to re-capture those fundamental effects [29].

As mentioned, the exchange and correlation energy of non-uniform electron density cannot be calculated exactly. However, any realistic system that is interesting for chemistry includes bonds or at least atoms, where the electron density is hardly uniform. Thus, similarly to Hartree–Fock theory, DFT also needs approximations to describe relevant models.

The first and most simple approximation is called the local density approximation. In local density approximation, the energy of the electron density in point r is found as the energy of a homogeneous electron gas of the same density [30]. This approximation is only accurate if the electron density varies slowly, as the captured effect is of local nature.

Another, a more viable approximation is called the gradient-generalized approximation (GGA). In GGA the inhomogeneities in the electron density are partially accounted for by including a factor, which depends on the local electron density gradient. Followingly, GGA density functionals are much more efficient in describing chemical bonding [31].

To improve upon GGA, a second derivative of the electron density is additionally included. Usually, the derivative of orbital kinetic energy is employed. The resulting functionals are called meta-GGA, and they are better at describing more diffuse bonds, where the exchange and correlation interactions are less localized [32, 33].

An alternative approach to improve a DFT method's performance is to mix it with a wavefunction theory method. The resulting functionals are the so-called hybrid functionals [34]. The most common example is combining the exact exchange energy from Hartree–Fock with that of DFT.

There exist novel double hybrid methods, that also include perturbation theory in the exchange–correlation functional to correct the correlation energy (*e.g.* B2PLYP which will be discussed further in section 3.1.1) [35]. Hybridization improves the performance of computations. In return, hybrid functionals are slower (double hybrid even more so), because they have to incorporate calculation steps that scale in 4th (or larger) order of the number of basis functions [14].

2.2 Estimated properties

The first property we estimated is the electrochemical stability of the ionic liquids corresponding to the studied ionic pairs. Previously, Ong *et al.*, Pandian *et al.* and others studied the electrochemical stability of ionic liquids with the help of DFT [36, 37]. The simplest approach is to correlate the cathodic stability with the LUMO energy value and the anodic stability with the HOMO energy value of ions forming an ionic liquid [36]. A more accurate approach relies on the delta self-consistent field (ΔSCF) method. In the ΔSCF method, the electron affinities (EA) and ionization energies (IE) are calculated from the electronic energy differences of reduced and oxidized species [36, 37].

The second property we estimated is viscosity. Viscosity is closely related to self-diffusion coefficient and ionic conductivity. Borodin *et al.* reported a correlation between the heat of vaporization (ΔH_{vap}), E_{int}, molar volume (V_{m}), self-diffusion coefficient (D), and ionic conductivity of 29 ionic liquids using molecular dynamics simulations [38]. In the following study, they suggested $\Delta H_{\mathrm{vap}} + 0.18E_{\mathrm{int}}$ as a descriptor of cohesive energy in an ionic liquid, which can be correlated to the average self-diffusion coefficient [39]. The proposed correlation applied more accurately for ionic liquids with similar packing and diffusion mechanism.

Bernard *et al.* observed a correlation between the melting point of an ionic liquid and the ratio of total E_{int} to its dispersion component. This relationship held true especially for the ionic liquids which shared an anion. Bernard *et al.* also noted that the dispersion component of E_{int} correlated better with viscosity and conductivity than the total E_{int}. The strong correlation between transport properties and dispersion interaction was explained by dispersion being disturbed the most by the diffusional movement of ions [40]. In this work we have correlated the viscosity of ionic liquids to the E_{int} and its dispersion component.

3 Methodology

In this chapter, the employed methods and models are discussed. First, the DFT functionals, corrections, and the reference computational method are introduced. Second, the simulation details are provided. Finally, the models used to estimate electrochemical stability and viscosity of the studied ionic pairs are defined.

3.1 Employed DFT functionals

3.1.1 B2PLYP

We used the B2PLYP functional to optimize all geometries. We chose B2PLYP as it was shown to be accurate for a variety of chemical systems [35]. However, being double hybrid means that the calculation time scales as the 5th order of the number of employed basis functions. B2PLYP uses Becke's 1988 exchange functional (B88) [41], the correlation functional by Lee–Yang–Parr (LYP) [34], Hartree–Fock exchange (HF), and the correlation from second-order perturbation theory (MP2) [42]:

$$E_{xc} = (1 - a_x)E_x^{\mathrm{B88}} + a_x E_x^{\mathrm{HF}} + (1 - c)E_c^{\mathrm{LYP}} + cE_c^{\mathrm{MP2}}, \tag{3.1}$$

where E_x denotes the exchange energy, E_c is the correlation energy, and the upper index determines the corresponding method. a_x and c are the scaling parameters, which are equal to 0.53 and 0.27 respectively. It is notable that the MP2 energy term is found directly using the Kohn–Sham orbitals [35].

3.1.2 SCAN and SCAN0

A recently developed exchange–correlation functional called SCAN was shown to have good accuracy when describing the energies and geometries of diversely bonded materials [24]. Furthermore, SCAN is the first meta-GGA functional that takes into account all 17 constraints that a meta-GGA should satisfy [23]. For this reason, differently from many other popular meta-GGA functionals, it is not fitted to experimental results. Thus, we decided to test for the first time if SCAN is a viable candidate for high-throughput screening of ionic liquids.

To reduce errors due to self- and non-covalent interactions, Hui and Chai proposed SCAN-based hybrid density functional called SCAN0. The functional mixes 75% of SCAN exchange energy with 25% of exchange energy from Hartree–Fock method [26]:

$$E_{\mathrm{xc}}^{\mathrm{SCAN0}} = E_{\mathrm{c}}^{\mathrm{SCAN}} + \frac{1}{4}E_{\mathrm{x}}^{\mathrm{HF}} + \frac{3}{4}E_{\mathrm{x}}^{\mathrm{SCAN}}. \tag{3.2}$$

Further testing by Hui and Chai showed that SCAN0 gave better results than its parent semi-local SCAN functional for a wide range of systems and therefore it can be categorized as hyper-GGA [26].

3.1.3 PBE and M06-L

To contrast the performance of SCAN we picked two popular non-hybrid functionals: PBE [31] and M06-L [43]. PBE, developed by Perdew–Burke–Ernzerfoh is one of the most widely used density functionals, which is known to yield acceptable results for most of chemical systems. M06-L, on the other hand, is a meta-GGA functional from the Minnesota 06 functionals family. After a systematic assessment by Zahn *et al.* they both were recommended for fast and accurate studies of the energetics of ionic liquid associates [14].

3.2 Corrections to DFT

Local density functional methods cannot properly describe the dispersion interaction [22]. To alleviate this systematic shortcoming, we employed the Grimme's long-range dispersion correction [25]. Furthermore, we rescaled the α_2 parameter for SCAN, as it has not been previously done.

Basis set incompleteness is an unavoidable problem throughout the whole quantum chemistry. Basis set is an arbitrary set of mathematical functions required to construct the electronic wave functions. Basis set superposition error occurs when the wave function belonging to a fragment is described by the wave function assigned to another fragment [44]. This effect is somehow similar to partial charge transfer, but it is not of physical origin and therefore artificially stabilizes the energy of the given fragments.

3.2.1 D3 dispersion correction

Grimme's dispersion correction (D3) was applied to correct the density functional methods in this work [25]. The London dispersion energy from the D3 scheme (E_{disp}) consists of the leading atom-pair wise term with Becke–Johnson (BJ) damping: [45–47]

$$E_{\text{disp}} = -1/2 \sum_{A}^{\text{atoms}} \sum_{B,B\neq A}^{\text{atoms}} \left[s_6 \frac{C_6^{AB}}{R_{AB}^6 + (a_1 R_{AB}^0 + a_2)^6} + s_8 \frac{C_8^{AB}}{R_{AB}^8 + (a_1 R_{AB}^0 + a_2)^8} \right]. \tag{3.3}$$

In this equation, C_n^{AB} denotes the nth-order dispersion coefficient for each atom pair AB, R_{AB} is their internuclear distance, and s_n are the order-dependent scaling factors. The cutoff radii $R_{AB}^0 = \sqrt{C_8^{AB}/C_6^{AB}}$ and a_1 and a_2 are fitting parameters, which depend on the employed functional.

3.2.2 Rescaling the SCAN D3 parameters

Brandenburg *et al.* used $\alpha_2 = 5.4200$, $s_6 = 1$, $s_8 = 0$ D3 parameters for SCAN and fitted the α_1 to be 0.5380 [48]. In our work, those parameters produced a systematic shift towards negative interaction energy values for SCAN corrected with D3 and CP (see below) (Figure 3.1). Thus, we rescaled both of the D3 damping parameters α_1 and α_2 to see whether we could eliminate the systematic errors. For that purpose, we considered α_1 values in the range of 0–1, and α_2 values in the range of 5–10 with a step of 0.05. The performance of SCAN+CP+D3 with different D3 parameters can be seen in Figure 3.1.

There is a clear linear dependence between α_1 and α_2 which is logical considering Equation 3.3.

Furthermore, Figure 3.1 does not reveal any steep energy minima, which made finding the optimal parameter values a non-trivial task. For the sake of simplicity, we decided to employ the α_1 value as fitted by Brandenburg *et al.* and found a α_2 value, which produces the lowest average mean absolute deviation in combination with this α_1.

Hence, the rescaled parameters are $\alpha_1 = 0.5380, \alpha_2 = 6.80$. Further D3 optimization was out of the scope of the current work. For certain SCAN will benefit from a more rigorous D3 optimization with a diversely bonded test set.

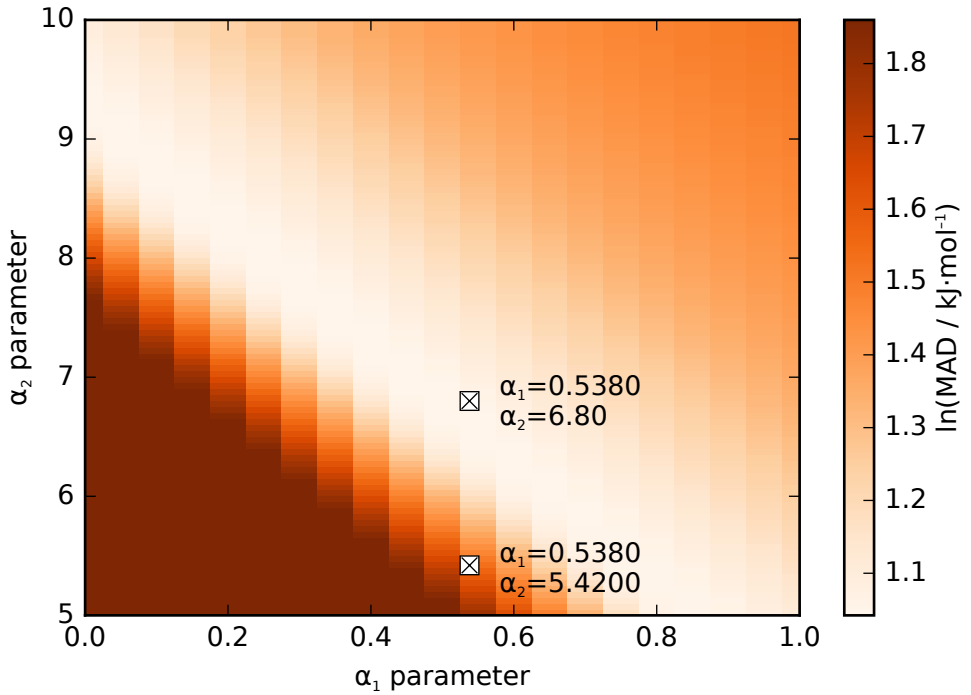

Figure 3.1: Average mean absolute deviation (MAD) of a counterpoise (CP) and dispersion (D3) corrected SCAN with varying Becke-Johnson damping parameters – α_1 and α_2 – for dispersion correction. The deviation scale is natural logarithmic and limited to 1.86 for better contrast. The pairs of α_1 and α_2 used in this work and by Brandenburg *et al.* are marked.

3.2.3 BSSE correction

As the exact basis sets for systems with more than one electron can not be known, certain errors stem from the incompleteness of the used basis sets. One of which is the BSSE, where the basis functions of one fragment artificially stabilize another fragment and *vice versa*. We have employed a Boys–Bernardi counterpoise scheme (CP) to reduce this error, which is defined as follows [27]:

$$E_{\text{counterpoise}} = E^{\text{cation}}_{\text{cation}} + E^{\text{anion}}_{\text{anion}} - (E^{\text{pair}}_{\text{cation}} + E^{\text{pair}}_{\text{anion}}), \tag{3.4}$$

where the lower index indicates the corresponding fragment and the upper index denotes the employed basis set. In other words, $E^{\text{cation}}_{\text{cation}}$ denotes the energy of the cation computed using the cation basis set, while $E^{\text{cation}}_{\text{pair}}$ denotes the energy of the cation computed using the basis set of the whole pair. The same logic applies to the anion. Note that all the single ions are also calculated on pair geometry throughout this work.

3.3 Reference method

CCSD(T) is the "gold standard" for modern quantum chemistry. However, it is also very expensive especially when paired with a large basis set. Thus, we have instead opted to use DLPNO-CCSD(T), an approximation to CCSD(T)-based method that yields a nearly identically accurate result [49].

The quality of wave function theory methods dramatically increases with the size of the employed basis set. As the basis set gets larger, the obtained energy converges to a limit [50–52]. To extrapolate the energy towards the complete basis set limit we used basis sets of different sizes. Herewith, we employed a cheaper SCS-MP2 method to extrapolate the energies, taking into account that the energy of SCS-MP2 converges at a similar rate [53].

3.3.1 Domain-based local pair natural orbital CCSD(T)

One way to drastically speed up the performance of CCSD(T) method is to localize the orbitals, which allows for faster electron correlation calculation. In local pair natural orbital CCSD(T) (LPNO-CCSD(T)) method, the localization is achieved by using a pair natural orbital for every electron pair. The pair natural orbitals are a highly compact set of orbitals that are different for each electron pair. This approach captures 99.5–99.7% of the correlation of CCSD(T), while the simplified orbitals improve the CPU scaling to the fifth power of system size [54].

The LPNO-CCSD(T) method was developed even further by Riplinger and Neese so that it would take more advantage of its local nature [49]. In domain-based local pair natural orbital CCSD(T) (DLPNO-CCSD(T)) each electron pair is assigned a domain of correlation, which allows neglecting many interactions while maintaining practically the same accuracy as LPNO-CCSD(T). Furthermore, in DLPNO-CCSD(T) the singles excitations energy is truncated [49].

The above approximations keep the DLPNO-CCSD(T) energies within one kcal/mol from those of CCSD(T) but make the calculation time scale almost linearly with the system size [13]. According to Ref. 55, DLPNO-CCSD(T) with tight parameters has less than 1 kJ/mol standard deviation from CCSD(T) for the FH dataset, [56] S66 database [57] and two datasets containing conformational energies of butane-1,4-diol [58] and melatonin [59]. For these reasons, we used DLPNO-CCSD(T) as a reference method in the current work.

3.3.2 Complete basis-set extrapolation

To obtain accurate electronic energies, one has to use large basis sets, which make even DLPNO-CCSD(T) calculations time-demanding. Fortunately, as the size of the basis set increases, the energies tend to converge smoothly towards complete basis set limit. This fact allows extrapolating the energies found with smaller basis sets to a near complete basis set energy [50–52]. We have extrapolated the correlation energy, and the self-consistent field (SCF) energy to the complete basis set (CBS) limit using spin-component scaled second-order Møller–Plesset perturbation theory (SCS-MP2) with Def2-TZVPP and Def2-QZVPP basis sets [60]:

$$
\begin{aligned}
E^{\mathrm{CBS}}_{\mathrm{correlation}} &= \frac{3^e E^{\mathrm{TZ}}_{\mathrm{correlation}} - 4^e E^{\mathrm{QZ}}_{\mathrm{correlation}}}{3^e - 4^e}, \\
E^{\mathrm{CBS}}_{\mathrm{SCF}} &= \frac{E^{\mathrm{TZ}}_{\mathrm{SCF}} - E^{\mathrm{QZ}}_{\mathrm{SCF}} e^{7.88(\sqrt{4}-\sqrt{3})}}{1 - e^{7.88(\sqrt{4}-\sqrt{3})}},
\end{aligned}
\tag{3.5}
$$

where E_Y^X denotes the energy of type X with basis set Y, and e stands for Euler's number. The factors 3 and 4 are derived from the amount of the split-valence basis functions used to describe a single orbital (ζ) (in Def2-TZVPP it is 3 and in Def2-QZVPP 4). Effective core potentials for iodine on the Def2-QZVPP level were employed [61]. The SCS-MP2 values found with equation 3.5 are then used in conjunction with the DLPNO-CCSD(T)/Def2-TZVPP results to extrapolate the latter towards the CBS limit:

$$E_{\mathrm{CCSD(T)}}^{\mathrm{CBS}} = E_{\mathrm{SCF}}^{\mathrm{CBS}} + E_{\mathrm{correlation}}^{\mathrm{CBS}} + (E_{\mathrm{CCSD(T)}}^{\mathrm{TZ}} - E_{\mathrm{SCS\text{-}MP2}}^{\mathrm{TZ}}). \tag{3.6}$$

According to Ref. 51 a similar approach, which includes the DLPNO approximation and uses MP2 results to extrapolate the DLPNO-CCSD(T) energies, has less than 2 kJ/mol mean deviation and less than 3 kJ/mol mean average deviation from the honestly extrapolated pure CCSD(T).

3.3.3 Spin-component scaled MP2

As described in the previous section, SCS-MP2 was employed instead of regular MP2 for extrapolating the DLPNO-CCSD(T) energies to the CBS limit. SCS-MP2 is a method developed from the second-order Møller–Plesset perturbation theory, where the correlation energy contributions from antiparallel- and parallel-spin pairs are viewed separately [53]. The antiparallel- and parallel-spin correlation energies in SCS-MP2 are scaled with two dimensionless factors respectively – the former slightly larger and the latter slightly smaller than unity:

$$E_{\text{scaled correlation}} = p_{\mathrm{S}} E_{\mathrm{S}} + p_{\mathrm{T}} E_{\mathrm{T}}, \tag{3.7}$$

where E_{S} and E_{T} are the correlation energy contribution from parallel-spin components ($\alpha\alpha, \beta\beta$) and the antiparallel-spin components respectively ($\alpha\beta, \beta\alpha$). The scaling factors were optimized by fitting them to benchmark reaction energies in Ref. 53 and established to be $p_{\mathrm{S}} = 1/3$ and $p_{\mathrm{T}} = 6/5$. The SCS-MP2 correlation energy is very similar to regular MP2, but the antiparallel-spin pair, singlet state is preferred. The described approach alleviates the tendency of MP2 to underestimate the extent to electron pairing [53].

3.4 Computation details

All calculations were run with Orca 3.0.3 unless stated otherwise [62]. The geometry optimization was done with Ahlrichs' type triple-ζ Def2-TZVPP basis set with polarization functions on all atoms [63, 64]. Tight self-consistent field convergence parameters, SCF integration grid 5 with final grid 6 and tight geometry optimization grids as defined in Orca 3.0.3 were used. The resolution of identity approximation was employed to speed up the calculations with approximations for Coulomb integrals, numerical Hartree–Fock exchange integrals, and MP2 correlation integrals. Grimme's dispersion correction with Becke–Johnson damping was also employed [25, 46, 47]. Most of the starting geometries were obtained from the Ref. 65 GitHub repository.

All single-point DFT calculations were performed on the B2PLYP optimized geometries. The single-point PBE, M06-L, and B2PLYP calculations were conducted using the Def2-TZVPP basis set, tight SCF convergence parameters, SCF integration grid 7, and the resolution of the identity approximation for Coulomb integrals as defined in Orca 3.0.3. For single-point B2PLYP calculations, the same RI-approximations were used as for the optimization. The Grimme's D3

dispersion correction was added to the final energies with Becke–Johnson damping [25,46,47]. Additionally, the Boys–Bernardi counterpoise correction procedure was used to account for the basis set superposition error (see sections 3.2.1 and 3.2.3 for details on the corrections) [27].

The SCAN calculations, as they were run with a modified version of Gaussian 03 code, employed 6-311++G(3df,3pd) basis set instead of Def2-TZVPP [66,67]. Herewith, for iodine, the diffuse functions were not included. Tight SCF convergence parameters and ultrafine SCF integration grids were employed as defined in Gaussian 03. Additionally, we calculated the D3 correction with parameters from Ref. 48 as well as with rescaled parameters (denoted D3*, rescaling is described in section 3.2.2), and the Gaussian 03 built-in Boys–Bernardi counterpoise correction. For selected ionic pairs, the hybrid version of SCAN with 25% of Hartree–Fock exchange (SCAN0) was also employed on the same basis set [26].

The DLPNO-CCSD(T) calculations are run with tight parameters ($T_{\mathrm{CutPairs}} = 10^{-5}, T_{\mathrm{CutPNO}} = 10^{-7}, T_{\mathrm{CutMKN}} = 10^{-4}$) and Def2-TZVPP basis set. The resolution of identity approximation was employed for the correlation integrals.

Spin-component scaled second-order Møller–Plesset perturbation theory (SCS-MP2) [53] calculations were run with both triple-ζ and quadruple-ζ split-valence basis sets (Def2-TZVPP and Def2-QZVPP), and resolution of the identity approximation for Coulomb and correlation integrals. Effective core potentials for iodine on the Def2-QZVPP level were employed [61]. The SCS-MP2 energies were used to extrapolate the DLPNO-CCSD(T) energies to the complete basis set limit.

3.5 Statistical methods

The main metrics for evaluating the performance of the functionals in this work are values of interaction energies and dipole moments. Interaction energy of an ionic pair is defined as:

$$E_{\mathrm{int}} = E_{\mathrm{ionic\ pair}} - (E_{\mathrm{cation}} + E_{\mathrm{anion}}), \tag{3.8}$$

where $E_{\mathrm{ionic\ pair}}$ denotes the electronic energy of the ionic pair, E_{cation} the electronic energy of the cation and E_{anion} the electronic energy of the anion (all at the optimized pair geometry). Interaction energies calculated with the DFT functionals were compared against the corresponding values obtained with the reference method – DLPNO-CCSD(T) extrapolated to the complete basis set limit.

To evaluate the performance of the functionals we used the following statistical parameters: maximum deviation (MAXD), mean absolute deviation (MAD), mean deviation or bias (MD), the standard deviation of error of predictions (SDEP), and correlation coefficient (r):

$$\mathrm{MAXD} = \max|D|, \qquad \mathrm{MAD} = \sum_{i=1}^{N}\frac{|D_i|}{N}, \qquad \mathrm{MD} = \sum_{i=1}^{N}\frac{D_i}{N},$$
$$\mathrm{SDEP} = \sqrt{\frac{1}{N}\sum_{i=1}^{N}(D_i - \bar{D}_i)^2}, \qquad r = \frac{\mathrm{cov}(Q_i, Q_i^{\mathrm{Ref.}})}{\sigma(Q)\sigma(Q^{\mathrm{Ref.}})}, \tag{3.9}$$

where N is the number of all ionic pairs in the dataset, $D_i = Q_i - Q_i^{\mathrm{Ref.}}$ stands for deviation, Q_i denotes a calculated quantity, while $Q_i^{\mathrm{Ref.}}$ represents the same quantity calculated using the

reference method. In the equation defining correlation coefficient r, cov is the co-variance between predicted and reference values, and σ stands for the standard deviation of the values.

The box-plot format is used for the presentation of results (Figures 4.2, 4.4A and 4.4B). In a box-plot the first and the third quartiles of the given dataset are represented by lower and upper box edges, the second quartile (. median) is represented by a horizontal line within a box, and the whiskers extend to the minimum and the maximum values. Outliers beyond 1.5 interquartile range of the box are portrayed separately, in which case the corresponding whisker is limited to ±1.5 interquartile range beyond the box.

3.6 Electrochemical stability

We have employed the ΔSCF method to estimate the electrochemical stability of ionic liquids based on the corresponding ionic pairs. In the ΔSCF method, the stability is assessed using the electron affinities (EA) and ionization energies (IE), which in turn are found from the electronic energy difference of oxidation and reduction processes respectively. The ionization energy (IE_{ion}) is mainly determined by the cation and thus defined as the difference between the electronic energies of the cation and its reduced form. Oppositely, electron affinity (EA_{ion}) is defined as the difference between the electronic energies of the anion and its oxidized form:

$$IE_{ion} = E(Cation^{+}) - E(Cation^{\bullet}), \qquad EA_{ion} = E(Anion^{-}) - E(anion^{\bullet}) \tag{3.10}$$

A more accurate model would require the inclusion of the solvation shell – either explicit or a continuum model to calculate the solvation energies for a complete thermodynamic cycle [68]. More expensive molecular dynamics simulation have also been shown to yield accurate results [37]. Furthermore, in molecular dynamics simulations, an electrode can be included in the system, which creates a more realistic environment for the decomposition.

However, in this work, the aim was to develop a model for predicting experimental properties with simple and robust DFT calculations, that can be scaled up to be employed in high-throughput screening (*e.g.* for the design and discovery of novel ionic liquids). For this reason, we did not consider molecular dynamics and used a modified ΔSCF method instead. Note, the ΔSCF method, which considers only single ions (Equation 3.10) tends to underestimate the overall electrochemical stability [37], because only ions in the vacuum are simulated, while important inter-ionic and interfacial interactions are neglected [69].

The inter-ionic interactions can, at first approximation, be included by additionally conducting the ΔSCF procedure with the whole ionic pair, which accounts for the solvation of an ion by its counter ion:

$$IE_{pair} = E(IP^{+}) - E(IP^{\bullet}), \qquad EA_{pair} = E(IP^{-}) - E(IP^{\bullet}) \tag{3.11}$$

By combining $0.25{\cdot}IE_{pair}$ with $0.75{\cdot}IE_{ion}$ and $0.25{\cdot}EA_{pair}$ with $0.75{\cdot}EA_{ion}$, the EAs and IEs for each ionic liquid were calculated. The scaling factors, 0.75 and 0.25, were obtained by fitting the calculated results against the experimental electrochemical stabilities (Table 6 in Reference [70]). The physical meaning of this scaling factor is closely related to the effective Madelung constant in the environment of decomposition (discussed in the Appendices). The employed approach includes an approximate solvation energy of the species involved in the redox reactions at the interface.

Found electron affinities and ionization energies of the ionic liquids are subsequently used to predict the electrochemical stabilities of the corresponding ionic liquids as represented by the electrochemical stability window (EW):

$$\mathrm{EW} = -\frac{\mathrm{EA} + \mathrm{IE}}{e} \tag{3.12}$$

3.7 Estimating viscosity

For energy applications of ionic liquids, one of the most interesting electrolyte properties is conductivity. This property is interrelated to diffusion coefficient and viscosity, see Appendices. In this study, we have estimated viscosity instead of diffusion coefficient or conductivity because there are more available experimental data on the former. Viscosity can be estimated readily with molecular dynamics simulations. However, the force fields in molecular dynamics do not describe electronic effects such as the charge transfer between ions, thus resulting in underestimated dynamics of ions and overestimated viscosity [71].

There are also three independent approaches for predicting viscosity: Quantum Structure–Property Relationship (QSPR), a Conductor-like Screening MOdel for Realistic Solvation (COSMO-RS), Volume-Based Thermodynamics (VBT) (see Refs. in [10]). All of them provide very good predictions, yet are extensively parametrized for specific families of anions and cations. The use of these approaches requires explorative studies for parametrization against very specific experimental data. Oppositely, the DFT-based model is used in this work to estimate viscosity in a more general way.

To avoid a time- and resource-consuming studies, instead of QSPR, COSMO-RS or VBT approach, we mix DFT calculations with pseudolattice formalism and transition state theory of reaction rates as follows.

In the 1940s Eyring *et al.* formulated viscosity as:

$$\eta = \frac{N_\mathrm{A} h}{V_\mathrm{m}} \exp\left(\frac{\Delta G}{RT}\right), \tag{3.13}$$

where N_A is the Avogadro's number, h is the Planck's constant, V_m is molar volume, R is the ideal gas constant, T denotes temperature, and ΔG is the energy of a diffusional jump [72]. More recently Han *et al.* further developed Eyring's formula 3.13 by taking into account the energy and the probability to create and occupy a hole in a liquid pseudolattice model [73].[a] For a non-polar liquid they arrived at:

$$\eta = \frac{N_a h}{V_\mathrm{m}} \exp\left(\frac{5.14\epsilon}{RT} - \frac{f}{2}\right), \tag{3.14}$$

where ϵ is the maximal Lennard–Jones potential between the particles and f is the number of degrees of freedom [73]. Lennard–Jones potential, however, is not sophisticated enough to accurately describe all interactions in ionic liquids. Thus, in this work, we correlate viscosities of ionic liquids to their interaction energies E_int and dispersion energies (E_disp) calculated with

[a] In Ref. 74 Abbott suggested an application of a similar hole theory to the viscosity of ionic and molecular liquids. His approach combines a formula for viscosity of an ideal gaseous medium with probability of finding a hole for a diffusional jump.

DFT. Furthermore, we neglect the factor f as it is expected to be of similar value for different ionic pairs, yielding:

$$\ln(\eta) = \ln(A) + E_a^{exp}/RT, \tag{3.15}$$

where A is a factor that depends on V_m.

3.7.1 Correlating activation energy

Firstly, we derived the activation energies of viscosity (E_a^{exp}) and the pre-exponent factors A from experimental viscosity–temperature dependencies for all of the ionic liquids that had said data available. The aforementioned parameters were calculated by linearizing the experimental viscosity (η) temperature dependence – according to Equation 3.15 the slope corresponds to E_a^{exp} and the intercept to A. Experimental viscosity–temperature dependence data were taken from the references listed in Table 5.1.

The E_a^{exp} were then correlated to the calculated E_{int} of corresponding ionic pairs. The latter were scaled by a coefficient a_i, which consists of a difference between two Madelung-type constants ($\Delta M = 0.165$) and the square of effective charge:

$$E_a^{est} = a_i E_{int} - bE_{disp} \tag{3.16}$$

where the normalization coefficients a_i and b are defined as follows:

$$a_i = -\Delta M q_i^2, \qquad b = -2\Delta M. \tag{3.17}$$

The effective charge (q) for ionic pairs was fitted by minimizing the root-mean-square deviation of the $E_{est} - E_{exp}$ dependence. q was found to be $0.85e$ and $0.74e$ for the ionic pairs with smaller and larger charge transfer (halides and cyanides, except $[B(CN)_4^-]$), respectively. The obtained q values are in agreement with the ionic charge values estimated using the CHELPG method (see Figure 4 in Ref. 75).

The dispersion energy (E_{disp}) was subtracted from the E_{int}, to describe the opposite effect of the dispersion forces on the diffusional movement of ions. The dispersion was scaled with coefficient b which was taken to be twice the ΔM value. In Ref. 75, b was originally half of ΔM, but the factor was increased to compensate for the fact that a portion of dispersion is included within B2PLYP due to the inclusion of MP2 correlation energy.

3.7.2 Correlating the pre-exponent factor *A*

As follows from Equation 3.14, A is inversely proportionate to V_m. It can be taken that the attractive component of dispersion interaction decays as the 6th power of distance and that the calculated dispersion energy value is determined mainly by the attractive component.[b] Hence, it can be roughly approximated that:

$$E_{disp} \propto -r^{-6} \propto -V_m^{-2} \Rightarrow V_m \propto \sqrt{\frac{1}{-E_{disp}}} \Rightarrow \ln(A) \propto \ln\left(\sqrt{-E_{disp}}\right). \tag{3.18}$$

The experimental A values were used to determine the slope and intercept of a linear correlation between $\ln(A)$ and $\ln(\sqrt{-E_{disp}})$ (slope $= 6.48$, intercept $= -24.91$). The ionic pairs with

[b] Curiosly, Bernard *et al.* also found that the dispersion component correlates well with viscosity.

larger partial charge transfer (halides and cyanides, except $[B(CN)_4^-]$) showed a different linear dependence. That effect may originate from stronger intermolecular interactions which alter the mechanism of diffusion. Alternatively, it could be related to the number of degrees of freedom or the pseudolattice parameters. For the sake of simplicity, the E_{disp} values for ionic pairs with larger partial charge transfer were multiplied by 2, which made them obey the same dependence as other ionic pairs.

Conclusively, by employing the proposed correlations and computing E_{int} and E_{disp}, the viscosity of ionic liquids that lack experimental data can be assessed. The degree of partial charge transfer can be used in applying the above mentioned correction in calculating a and A. By substituting Equation 3.16 and the solution from Equation 3.18 into Equation 3.15 we obtain:

$$\ln(\eta^{\mathrm{est}}) = 6.48 \cdot \ln\left(\sqrt{-E_{\mathrm{disp}}}\right) - 24.91 + \frac{a_i E_{\mathrm{int}} - bE_{\mathrm{disp}}}{RT}. \tag{3.19}$$

4 Results

The studied set of 48 ionic pairs is composed of commonly used ionic liquid anions and cations. The list of anions includes halide, cyanide, borate, sulphonate, phosphate, and imide-based anions; the list of cations includes N,N,N-triethyl-N-propylammonium, 1-butylpyridinium, 1-butyl-1-methylpyrrolidinium, 1-butyl-3-methylimidazolium cations (Figure 4.1).

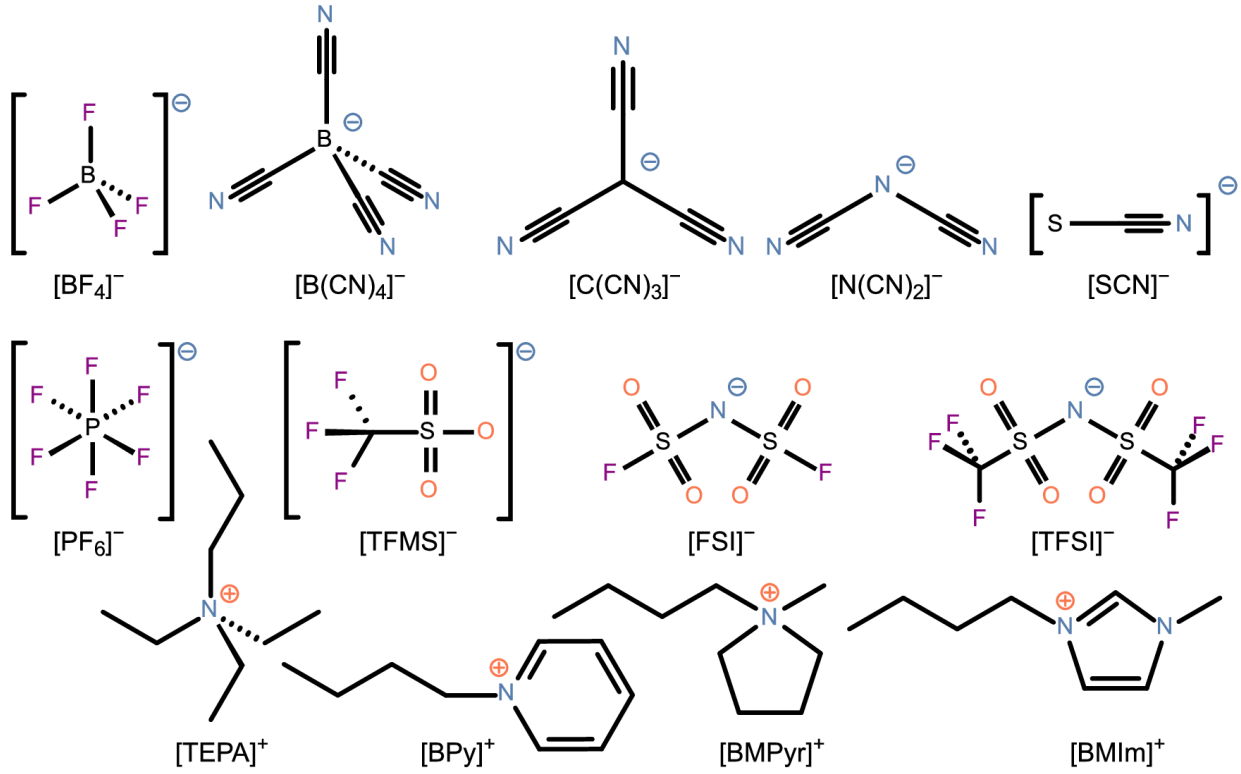

Figure 4.1: 2D structural formulas of the anions and the cations used to combine ionic pairs. From the top left: tetrafluoroborate, tetracyanoborate, tricyanomethanide, dicyanamide, isothiocyanate, hexafluorophosphate, trifluoromethylsulfonate, bis-(fluorosulfonyl)imide, bis-[(trifluoromethyl)sulfonyl]imide, N,N,N-triethyl-N-propylammonium, 1-butylpyridinium, 1-butyl-1-methylpyrrolidinium, 1-butyl-3-methylimidazolium. Chloride, bromide and iodide ions were also employed but are not shown in the Figure.

After the geometry optimization using B2PLYP functional, the anion and cation in each ionic pair ended up relatively close to each other. The distances between the geometric centers of the two are in the range between 2.7 Å in the case of 1-butyl-3-methylimidazolium chloride, and 5.1 Å for N,N,N-triethyl-N-propylammonium bis[(trifluoromethyl)sulfonyl]imide. At the DLPNO-CCSD(T) level of theory, the majority of the ionic pairs has dipole moment around 5 D.

The smallest dipole moment of 2.8 D has 1-butylpyridinium chloride, while the largest dipole moment of 7.3 D belongs to N,N,N-triethyl-N-propylammonium tetracyanoborate. As follows from the DLPNO-CCSD(T) calculations, the majority of ionic pairs has the interaction energy between −380 kJ/mol and −340 kJ/mol. The most weakly associated ionic pair in the dataset is N,N,N-triethyl-N-propylammonium tetracyanoborate (E_{int} = −291 kJ/mol), while the most strongly bound ionic pair is 1-butylpyridinium chloride (E_{int} = −410 kJ/mol). The ionic pair interaction energy characterizes the cohesion of ionic liquids. It is related to properties such as viscosity, diffusion coefficients, and surface tension [38, 40, 75]. It also serves as an attractive benchmark metrics, since it is reasonable to suggest that DFT functionals capable of predicting interaction energies of ionic pairs will be able to accurately predict the cohesion in bulk ionic liquids and at interfaces.

Distributions of distances between the ions, dipole moments, and interaction energies are provided in the Appendices (Figure 5.1, Table 5.2). The whole dataset along with the optimized geometries is available at GitHub (see Ref. 76). The DLPNO-CCSD(T) reference data have been used to benchmark the performance of SCAN and other density functionals. The B2PLYP results were used to estimate the stability and viscosity of the ionic liquids corresponding to these ionic pairs.

4.1 Performance of the tested DFT functionals

The performance of the tested functionals for estimating the interaction energies is shown in Figure 4.2. For the sake of clarity, we show only the best performing approach(es) for each functional.

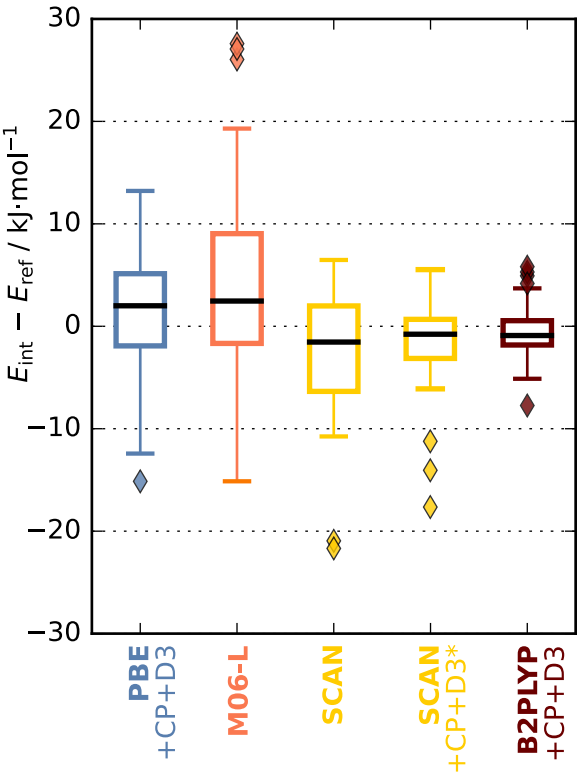

Figure 4.2: The distribution of errors in interaction energies (relative to the reference method) for the employed DFT methods with the most relevant corrections.

Interaction energies obtained with B2PLYP are very close to those of the reference method and surpass all other employed methods in accuracy. B2PLYP, however, contains contributions from MP2, so it is also considerably slower than the other methods. Furthermore, the fact that the geometries were optimized on the B2PLYP/Def2-TZVPP level skews the results in its favor.

In Figure 4.2, one can also see that errors within SCAN+CP+D3* functional are quite systematic, with the majority falling into −3 to 1 kJ/mol range. The other methods presented in Figure 4.2 also have smaller than 5 kJ/mol median error, but the distributions of errors are considerably larger, with the most dramatic case, M06-L (within −10 to 20 kJ/mol range).

It is worth separately addressing the effects of employed corrections. The counterpoise (CP) corrects the basis set superposition error (typically positive), while the dispersion correction (D3) improves the inadequate description of dispersion interactions (typically negative). These errors are common to the majority of the DFT methods. The functionals performance with and without the different corrections is demonstrated in Table 4.1. When CP and D3 are applied, they improve the mean absolute deviation (MAD) of both PBE and B2PLYP, as well as decrease the standard deviation of error of prediction (SDEP) in the case of SCAN. Using D3* with the rescaled parameters further decreases the deviations of CP-corrected SCAN.

Functional	Basis set	MAXD kJ/mol	MAD kJ/mol	MD kJ/mol	SDEP kJ/mol
PBE	Def2-TZVPP	32.8	17.0	14.6	12.0
PBE+D3	Def2-TZVPP	32.5	7.0	−6.5	7.0
PBE+CP	Def2-TZVPP	40.1	22.8	22.6	9.3
PBE+D3+CP	Def2-TZVPP	**15.1**	**4.7**	**1.6**	**5.8**
M06-L	Def2-TZVPP	27.6	**7.6**	**3.7**	**9.5**
M06-L+D3	Def2-TZVPP	85.3	31.3	−20.6	26.8
M06-L+CP	Def2-TZVPP	75.7	33.7	−25.5	25.3
M06-L+D3+CP	Def2-TZVPP	**23.1**	10.2	4.8	10.3
SCAN	6-311++G(3df,3pd)	21.7	4.9	−2.4	6.2
SCAN+D3	6-311++G(3df,3pd)	25.3	10.4	−10.1	5.3
SCAN+D3*	6-311++G(3df,3pd)	23.9	7.6	−7.2	5.4
SCAN+CP	6-311++G(3df,3pd)	**16.0**	4.9	2.9	5.2
SCAN+D3+CP	6-311++G(3df,3pd)	19.0	5.2	−4.9	**3.9**
SCAN+D3*+CP	6-311++G(3df,3pd)	17.7	**2.9**	**−1.9**	4.1
B2PLYP	Def2-TZVPP	23.1	10.2	4.8	10.3
B2PLYP+D3	Def2-TZVPP	36.1	11.9	−11.9	7.5
B2PLYP+CP	Def2-TZVPP	25.2	16.3	16.3	5.1
B2PLYP+D3+CP	Def2-TZVPP	**7.7**	**2.1**	**−0.5**	**2.7**

Table 4.1: The performance of the studied functionals against the reference method. Bold characters mark the smallest MAXD, MAD, MD and SDEP values for each functional.

4.1.1 Detailed evaluation of the SCAN results

As can be seen in Table 4.1, while SCAN+D3+CP shows smaller SDEP than the pure SCAN, it is also slightly less accurate. In other words, SCAN+D3+CP is more precise, but interaction

energies are systematically biased to be more negative than the corresponding reference values as described by the relatively large negative mean deviation (MD of −5 kJ/mol). It is possible that D3 over-corrects the SCAN interaction energies. This effect might originate from the fact that SCAN is a meta-GGA functional that implicitly includes mid-range dispersion interactions. Here we used SCAN D3 parameters taken from the Ref. 48. However, the authors of that publication optimized only a single D3 parameter, α_1. Therefore, we rescaled damping parameters α_1 and α_2, which control how the dispersion interaction decays over distance (see section 3.2.2 for details). The rescaled D3* along with CP-correction eliminates the systematic shift and produces significantly smaller deviations as can be seen in Table 4.1.

In Figure 4.3 the SCAN+CP+D3* interaction energies for each pair of ions are plotted against their corresponding reference values; PBE+CP+D3 and M06-L data points are added for contrast. A similar graph with distinguishable data-points for individual ionic pairs calculated with SCAN+CP+D3* is given in the Appendices (Figure 5.2). While the overall agreement of the corrected SCAN and the reference method is good, it can be seen that larger deviations occur for some of the more strongly interacting ionic pairs. Note that the same outliers also appear for PBE+CP+D3 and M06-L.

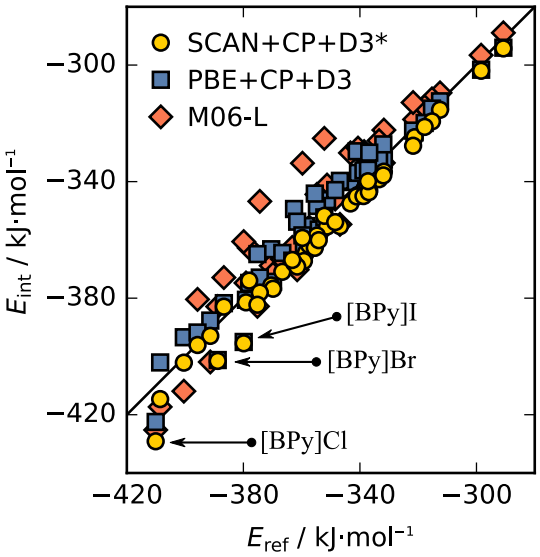

Figure 4.3: The performance of the tested functionals relative to the reference method.

The three biggest outliers for the SCAN+CP+D3* method are all 1-butylpyridinium halides (chloride, bromide, and iodide) as specified in Figure 4.3. This likely occurs due to the self-interaction error – an interaction of an electron with itself that is present in approximate DFT methods [77]. To avoid this error, we have also calculated the halide anion-containing ionic pairs with SCAN0 [26]. This hybrid functional includes a Hartree–Fock contribution that negates the effects of the self-interaction error. In ionic associates, the self-interaction error leads to an artificial increase of partial charge transfer between the ions [78]. That is why it is most severe for ionic pairs with 1-butylpyridinium cation, as those ionic pairs have the largest partial charge transfer due to the proximity of HOMO and LUMO (see Ref. 75). Increased partial charge transfer directly leads to overestimated interaction energies and underestimated dipole moments.

However, application of SCAN0 for the halide anion-containing ionic pairs improves the results. This can be judged by examining the distribution of obtained errors in interaction energies shown in Figure 4.4A. Note that due to D3 being unparametrized for SCAN0, no D3 correction was

added to the respective energies. It can be seen that compared to SCAN and SCAN+CP+D3*, SCAN0 predicts the interaction energies for halide anion-containing ionic pairs more accurately. We conclude that the hybridization with the exact exchange or self-interaction correction is necessary for systems where there is a large extent of partial charge transfer.

For comparison, in Figure 4.4B we displayed the performance of the functionals for all ionic pairs that do not contain halide anions. The results are similar to those seen in Figure 4.2A, but with higher accuracy and without the outliers. These findings suggest that ionic liquids excluding chlorides, bromides, and iodides can be effectively studied using the SCAN density functional.

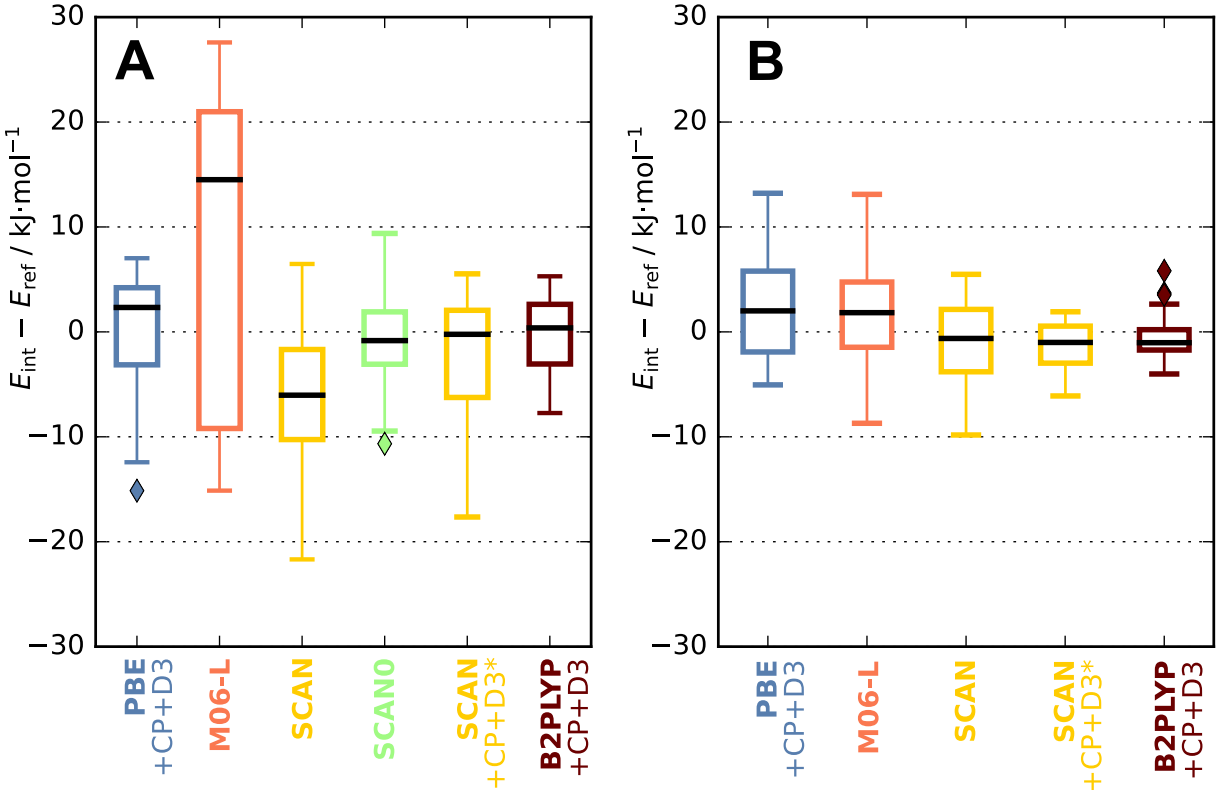

Figure 4.4: The distribution of errors in interaction energies (relative to the reference method) for the employed DFT methods. Plot a is for the halide-containing ionic pairs. Plot B contains all but halides.

4.1.2 The comparison of the description of dipole moments

Table 4.2 provides a comparison of calculated dipole moments. Note that neither CP nor D3 corrections affect the electronic structure. For this reason, they are omitted. All predictions are accurate in comparison to the DLPNO-CCSD(T) results, with r^2 even for the worst method exceeding 0.99. The table suggests that while SCAN functional predicts magnitudes of dipole moments better than PBE, it gives slightly larger errors compared to M06-L and B2PLYP.

Comparison of the results obtained using the SCAN and M06-L functionals presents an interesting contradiction: SCAN produces a greater error in the calculation of dipole moments but more accurate interaction energies. This indicates that M06-L describes charge transfer better than SCAN but incorrectly estimates its energetic effect. The relatively good performance of M06-L even in comparison with hybrid functionals was seen in the work of Lage-Estebanez *et al.*, [79]

where authors related the charge transfer to the self-interaction error. So, we concluded that the self-interaction error correction could be used to improve the overall SCAN performance.

Earlier Perdew suggested that there are two roads to follow to alleviate the self-interaction error [80]. One is to apply the Perdew–Zunger self-interaction error correction to a pure DFT functional, [77] and the other one is to use hybrid functionals, such as SCAN0. In this work, we tested the second road, leaving the first one for a separate study. It can be seen in Table 4.3 that SCAN0 surpasses all of the studied non-hybrid functionals in accuracy and rivals the double-hybrid B2PLYP.

Error	PBE	SCAN	M06-L	B2PLYP
MAXD	−0.505	−0.381	**−0.358**	−0.108
MAD	0.216	0.131	**0.110**	0.043
MD	−0.216	−0.131	**−0.110**	−0.036
SDEP	0.087	0.075	**0.064**	0.038
r^2	0.993	0.994	0.995	0.998

Table 4.2: The deviations of the magnitude of dipole moments in Debye for the studied functionals. The smallest error values among the non-hybrid functionals are marked by bold.

Error	PBE	SCAN	SCAN0	M06-L	B2PLYP
MAXD	−0.489	−0.325	**−0.129**	−0.282	0.109
MAD	0.331	0.120	**0.056**	0.150	0.033
MD	−0.331	−0.120	**−0.015**	−0.150	0.021
SDEP	0.077	0.099	**0.068**	0.069	0.038
r^2	0.996	0.995	0.996	0.996	0.998

Table 4.3: The deviations of the magnitude of dipole moments in Debye for the studied functionals when describing halide containing ionic pairs. The smallest error values among the non-hybrid functionals and SCAN0 are marked by bold.

4.2 Prediction of physicochemical properties

The electrochemical stability and viscosity were estimated for the same 48 ionic liquids. Although high-throughput screening with B2PLYP is improbable, in this work, we used B2PLYP results. Our main focus was on the development of the model for prediction of the physicochemical properties of ionic liquids. Our goal was to obtain the correct relative ranking of ionic liquids rather than accurately reproduction of the experimental values *per se*. In future, we aim to reproduce the estimations with SCAN functional as well as to use SCAN for high-throughput screening in search for ionic liquids with desirable properties.

4.2.1 Electrochemical stability

Stability is one of the most important properties of ionic liquids in electrochemical applications. The ΔSCF method, described in section 3.6, enables estimating the IE and EA values that can

be used to estimate the electrochemical stability windows. EA and IE values were calculated for 48 ionic pairs; they are shown in Figure 4.5.

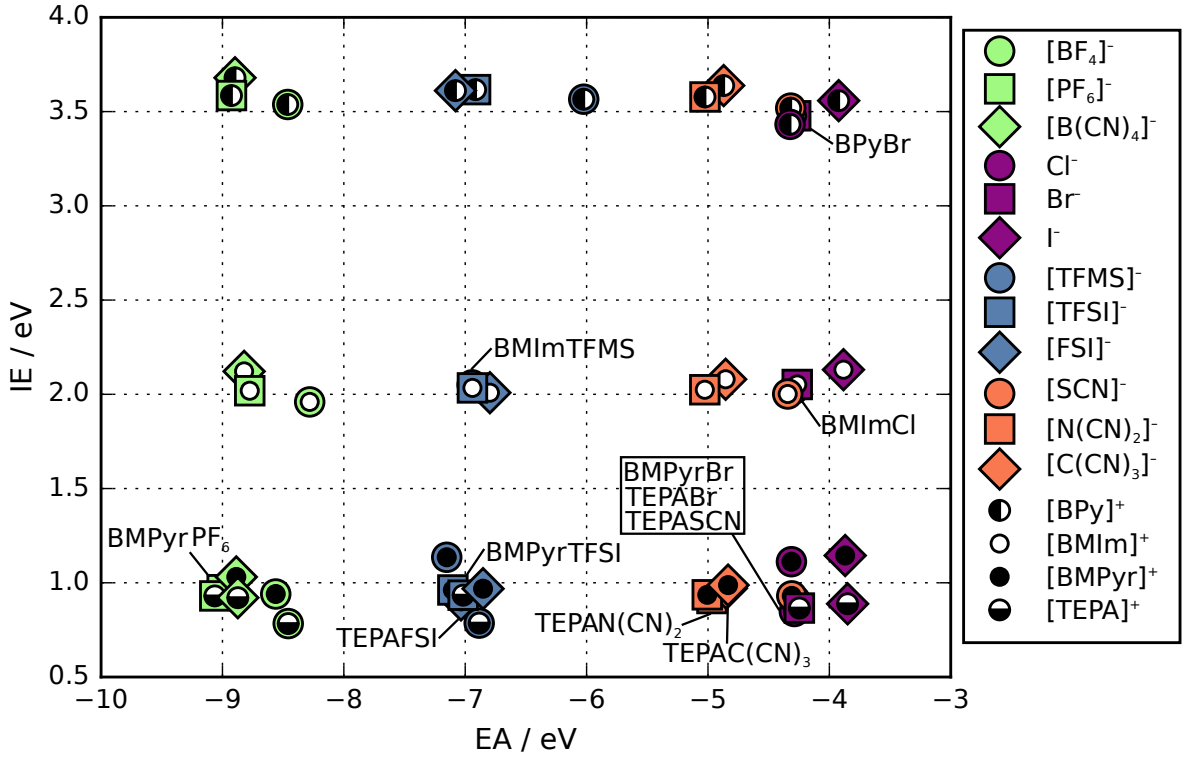

Figure 4.5: Electron affinities and ionization energies of 48 ionic pairs, determined with the ΔSCF method. Each of the inner circles indicates a cation, and the surrounding marker indicates an anion of an ionic pair.

Figure 4.5 provides the relative stabilities of the studied ionic pairs – lower IE corresponds to stability towards reduction and lower EA corresponds to stability towards oxidation. Therefore, in Figure 4.5 the most stable ionic pairs reside in the bottom left. An approach that can reproduce experimental stabilities on an absolute scale would require modeling of the interface as well as explore all possible reaction pathways, which would make the simulations more complicated and less scalable. However, the employed DFT method yields the relative stability ranking for ions: $[TEPA]^+ \approx [BMPyr]^+ > [BMIm]^+ > [BPy]^+$ and $[PF_6]^- > [B(CN)_4]^- > [BF_4]^- > [TFSI]^- > [FSI]^- \approx [TFMS]^- \gg [N(CN)_2]^- \approx [C(CN)_3]^- > Cl^- > Br^- \approx [SCN]^- > I^-$, which is in qualitative agreement with the experiment (see Refs in 1).

4.2.2 Viscosity

The computational and experimental activation energies of viscosity and coefficients A were evaluated as described in Section 3.7. In Figure 4.6A the relation between the normalized interaction energy (E_a^{est}, Equation 3.16) and the activation energy of viscosity (E_a^{exp}, slope from linearizing Equation 3.15) is shown. The r^2 between E_a^{est} and E_a^{exp} was 0.85; when deriving E_a^{exp} from the experimental viscosity–temperature dependences, the r^2 values were all above 0.99. In Figure 4.6B the relation between the dispersion energy (E_{disp}, from Grimme's dispersion correction) and the experimental coefficient A (intercept from linearizing Equation 3.15) is shown. The r^2 in Figure 4.6B is 0.90.

Combined, the correlations to estimate A and E_a based on E_{int} and E_{disp} are used to computationally evaluate the viscosity. The developed DFT-based model (Equation 3.19), though approximate, represents a quick and robust way of estimating the parameters necessary to determine the viscosity of a pure ionic liquid.

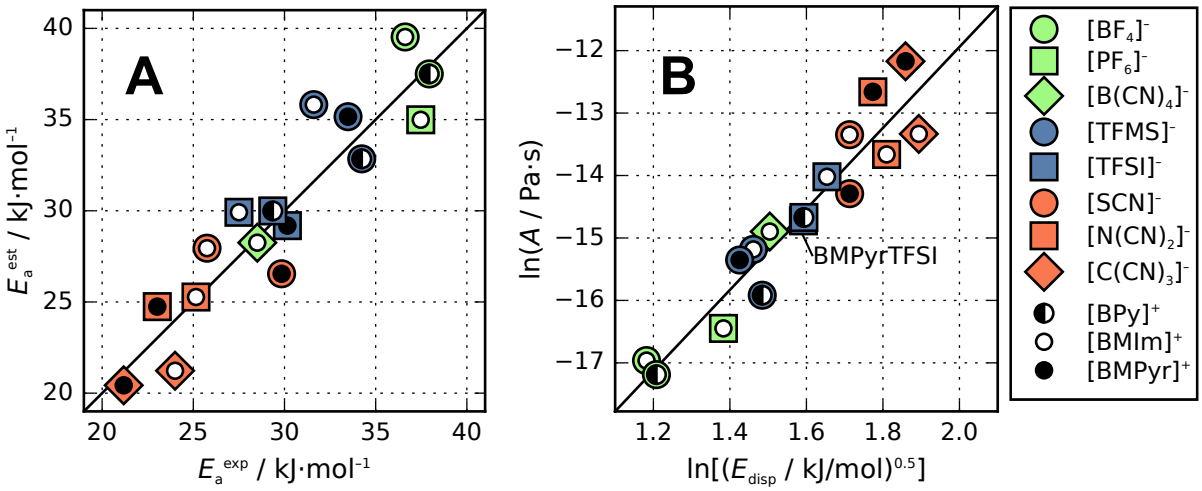

Figure 4.6: A: The relation between the estimated E_a^{est} and the experimental E_a^{exp} activation energy of viscosity. B: The relation between the factor A and dispersion interaction. Each of the inner circles indicates a cation, and the surrounding marker indicates an anion of an ionic pair.

4.2.3 Stability–viscosity trend and future work

In Figure 4.7, the computationally estimated viscosity (Equation 3.19) is plotted against the calculated electrochemical stability windows (Equation 3.12) of the studied ionic pairs. The more stable ionic liquids, such as those containing the $[BF_4]^-$ and $[PF_6]^-$, are known to be very viscous, while the less stable ionic liquids (*e.g.* those with cyanide-based anions) appear to have lower viscosities. Ionic pairs containing halide anions have higher viscosity due to their strong interaction energy and are also quite unstable. The ionic pairs with $[TFSI]^-$, $[FSI]^-$, and $[TFMS]^-$ anions appear to be moderately stable (unless paired with 1-butylpyridinium cation) as well as moderately viscosity.

Ionic pairs with $[C(CN)_3]^-$, $[N(CN)_2]^-$ anions give ionic liquids that are presumably less electrochemically stable but have low viscosities. On the other hand, $[B(CN)_4]^-$ containing ionic pairs show the most promising results by being both among the most stable and the least viscous of the considered ionic pairs.

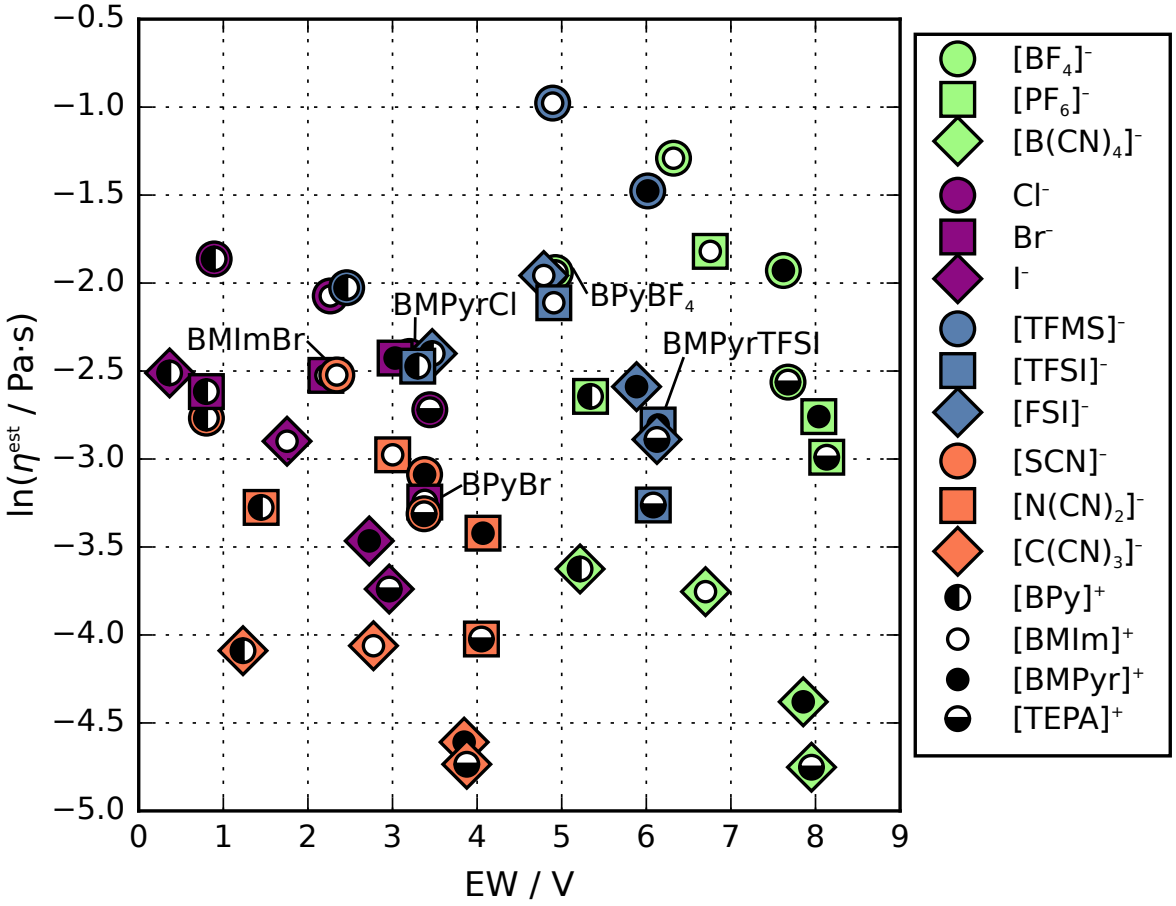

Figure 4.7: The relation between the electrochemical stability window (EW) and the estimated viscosity (η^{est}). Each of the inner circles indicates a cation, and the surrounding marker indicates an anion of an ionic pair.

Wide electrochemical stability window and low viscosity as well as high conductivity are highly desirable characteristics for batteries and supercapacitors. Subsequently, we conclude that the ionic liquids with "good" predicted properties could be successfully utilized in various electrochemical applications. Indeed, ionic liquids with $[TFSI]^-$, $[FSI]^-$, $[C(CN)_3]^-$, $[N(CN)_2]^-$, and $[B(CN)_4]^-$ anions were previously proposed and successfully tested as potential electrolytes [1, 2].

For example, 1-ethyl-3-methylimidazolium tetracyanoborate as an electrolyte for the supercapacitor was shown to possess remarkable properties [81]. Moreover, under overvoltage conditions, electrochemical energy storage device containing tetracyanoborate anions in the electrolyte does not explode due to a self-blocking mechanism (formation of polycyanoborani polymer) [82].

$Li[B(CN)_4]$ in $[BMPyr][B(CN)_4]$ as an electrolyte for Li-ion batteries demonstrated better cycling stability than $Li[BF_4]$ salt [83]. Unfortunately, the lithium salt solubility in $[BMPyr][B(CN)_4]$ is too low [83–85]. Yet, $Li[N(CN)_2]$ and $Li[C(CN)_3]$ as well as $Na[B(CN)_4]$ are soluble in the corresponding pyrrolidinium-based ionic liquids [83, 84]. Note, that Li^+ is well soluble in ionic liquids containing $[TFSI]^-$, $[FSI]^-$, and $[TFMS]^-$ anions due to the presence of oxygen atoms which coordinates with lithium. However, the coordination has a disturbing effect on the Li^+ transport properties of the electrolytes. In this respect, non-fluorinated ionic liquids with cyano-based anions possess lower viscosity and higher conductivity. They exhibit a fairly low

toxicity [86], and can also be manufactured relatively inexpensively [84].

Thence, by analyzing stability–viscosity trend (as shown in Figure 4.7) it is possible to choose the most suitable candidates for a given practical application. We believe that the developed DFT-based model can be used in the high-throughput screening of ionic liquids even before their experimental evaluation. In the future work, we plan to test this hypothesis by broadening the dataset of ionic liquids. We also plan to enlarge the studied models from ionic pairs to larger associates to predict melting point values using pseudolattice formalism as described in Ref. 87. Finally, we are planning to utilize novel SCAN functional (instead of B2PLYP) to speed-up all related calculations.

5 Summary

In this work, we have evaluated the performance of the recently proposed strongly constrained and appropriately normed (SCAN) density functional on a set of 48 ionic liquid pairs. The main focus was on the interaction energies and dipole moments; their predictions with SCAN have been compared to the values of DLPNO-CCSD(T) and other DFT methods. Our key findings are the following:

- More accurate interaction energies for SCAN are obtained in combination with Grimme's D3 dispersion correction and Boys–Bernardi counterpoise (CP) corrections. The mean absolute deviation of the SCAN+D3+CP functional for our dataset is 2 kJ/mol.
- SCAN+D3+CP is a fast and accurate method for evaluating interaction energetics of ionic liquid associates. It can be utilized in both high-throughput screenings as well as DFT-based molecular dynamics simulations.
- SCAN might be sensitive to the self-interaction error, which is demonstrated in the example of ionic pairs containing chloride, bromide, and iodide anions.

Next, we report a correlation between the interaction energy of an ionic pair and the viscosity of the corresponding ionic liquid. This correlation serves as an example of how DFT can be utilized to predict not only the static but also the dynamic properties. Furthermore, with the help of DFT, we evaluated the relative electrochemical stability of ionic liquids. In sum, we have developed a DFT-based model allowing a quick yet efficient screening of ionic liquids for desirable viscosity and electrochemical stability values. The model can be used for qualitative assessment of large datasets. Thus, it can help in searching for promising candidates among diverse classes of ionic liquids for energy applications.

Acknowledgements

I would like to express my gratitude to my supervisors – Meeri Lembinen and Vladislav Ivaništšev – for their support, continuous positive mental attitude and knowledge that were necessary to complete this thesis. I am also grateful to Maksim Mišsin for providing invaluable insight and stimulating discussion.

References

[1] M. V. Fedorov, A. A. Kornyshev, Ionic liquids at electrified interfaces, Chem. Rev. 114 (5) (2014) 2978–3036.

[2] D. R. MacFarlane, N. Tachikawa, M. Forsyth, J. M. Pringle, P. C. Howlett, G. D. Elliott, J. H. Davis, M. Watanabe, P. Simon, C. A. Angell, Energy applications of ionic liquids, Energy Environ. Sci. 7 (2014) 232–250.

[3] N. V. Plechkova, K. R. Seddon, Applications of ionic liquids in the chemical industry, Chem. Soc. Rev. 37 (1) (2008) 123–150.

[4] E. I. Izgorodina, Towards large-scale, fully ab initio calculations of ionic liquids, Phys. Chem. Chem. Phys. 13 (10) (2011) 4189–4207.

[5] T. Husch, M. Korth, Charting the known chemical space for non-aqueous lithium-air battery electrolyte solvents, Phys. Chem. Chem. Phys. 17 (35) (2015) 22596–22603.

[6] T. Husch, M. Korth, How to estimate solid-electrolyte-interphase features when screening electrolyte materials, Phys. Chem. Chem. Phys. 17 (35) (2015) 22799–22808.

[7] T. Husch, N. D. Yilmazer, A. Balducci, M. Korth, Large-scale virtual high-throughput screening for the identification of new battery electrolyte solvents: computing infrastructure and collective properties, Phys. Chem. Chem. Phys. 17 (5) (2015) 3394–3401.

[8] C. Schütter, T. Husch, M. Korth, A. Balducci, Toward new solvents for EDLCs: from computational screening to electrochemical validation, J. Phys. Chem. C 119 (24) (2015) 13413–13424.

[9] M. Korth, Large-scale virtual high-throughput screening for the identification of new battery electrolyte solvents: evaluation of electronic structure theory methods, Phys. Chem. Chem. Phys. 16 (17) (2014) 7919–7926, 00003.

[10] E. I. Izgorodina, Z. L. Seeger, D. L. A. Scarborough, S. Y. S. Tan, Quantum chemical methods for the prediction of energetic, physical, and spectroscopic properties of ionic liquids, Chem. Rev.

[11] R. Hayes, G. G. Warr, R. Atkin, Structure and nanostructure in ionic liquids, Chem. Rev. 115 (13) (2015) 6357–6426, PMID: 26028184.

[12] J. Řezáč, P. Hobza, Describing noncovalent interactions beyond the common approximations: How accurate is the "Gold standard," CCSD(T) at the complete basis set limit?, J. Chem. Theory Comput. 9 (5) (2013) 2151–2155, PMID: 26583708.

[13] D. G. Liakos, F. Neese, Is it possible to obtain coupled cluster quality energies at near density functional theory cost? domain-based local pair natural orbital coupled cluster vs modern density functional theory, J. Chem. Theory Comput. 11 (9) (2015) 4054–4063.

[14] S. Zahn, D. MacFarlane, E. I. Izgorodina, Assessment of kohn-sham density functional theory and moller-plesset perturbation theory for ionic liquids, Phys. Chem. Chem. Phys. 15 (2013) 13664–13675.

[15] E. I. Izgorodina, U. L. Bernard, D. R. MacFarlane, Ion-pair binding energies of ionic liquids: Can DFT compete with ab initio-based methods?, J. Phys. Chem. A 113 (25) (2009) 7064–7072.

[16] R. G. Parr, W. Yang, Density Functional Theory of Atoms and Molecules, Oxford University Press, New York, 1989.

[17] A. D. Becke, Perspective: Fifty years of density-functional theory in chemical physics, J. Chem. Phys. 140 (18) (2014) 18A301.

[18] J. P. Perdew, K. Schmidt, V. Van Doren, C. Van Alsenoy, P. Geerlings, Jacob's ladder of density functional approximations for the exchange-correlation energy, in: AIP Conference Proceedings, Vol. 577, AIP, 2001, p. 1–20.

[19] B. Kirchner, O. Hollóczki, J. N. Canongia Lopes, A. A. H. Pádua, Multiresolution calculation of ionic liquids, Wiley Interdiscip. Rev. Comput. Mol. Sci. 5 (2) (2015) 202–214.

[20] M. Salanne, Simulations of room temperature ionic liquids: from polarizable to coarse-grained force fields, Phys. Chem. Chem. Phys. 17 (2015) 14270–14279.

[21] N. Marom, A. Tkatchenko, M. Rossi, V. V. Gobre, O. Hod, M. Scheffler, L. Kronik, Dispersion interactions with density-functional theory: Benchmarking semiempirical and interatomic pairwise corrected density functionals, J. Chem. Theory Comput. 7 (12) (2011) 3944–3951.

[22] S. Grimme, W. Hujo, B. Kirchner, Performance of dispersion-corrected density functional theory for the interactions in ionic liquids, Phys. Chem. Chem. Phys. 14 (14) (2012) 4875–4883.

[23] J. Sun, A. Ruzsinszky, J. P. Perdew, Strongly constrained and appropriately normed semilocal density functional, Phys. Rev. Lett. 115 (3) (2015) 036402.

[24] J. Sun, R. C. Remsing, Y. Zhang, Z. Sun, A. Ruzsinszky, H. Peng, Z. Yang, A. Paul, U. Waghmare, X. Wu, M. L. Klein, J. P. Perdew, Accurate first-principles structures and energies of diversely bonded systems from an efficient density functional, Nat. Chem. 8 (2016) 831–836.

[25] S. Grimme, J. Antony, S. Ehrlich, H. Krieg, A consistent and accurate ab initio parametrization of density functional dispersion correction (DFT-D) for the 94 elements h-pu, J. Chem. Phys. 132 (2010) 154104.

[26] K. Hui, J.-D. Chai, SCAN-based hybrid and double-hybrid density functionals from models without fitted parameters, J. Chem. Phys. 144 (4) (2016) 044114.

[27] S. F. Boys, F. Bernardi, The calculation of small molecular interactions by the differences of separate total energies. some procedures with reduced errors, Mol. Phys. 19 (4) (1970) 553–566.

[28] H. Kruse, S. Grimme, A geometrical correction for the inter- and intra-molecular basis set superposition error in hartree-fock and density functional theory calculations for large systems, J. Chem. Phys. 136 (15) (2012) 154101.

[29] K. Burke, The ABC of DFT, Department of Chemistry, University of California, 2007.

[30] W. Kohn, L. J. Sham, Self-consistent equations including exchange and correlation effects, Phys. Rev. 140 (4A) (1965) 1133–1138.

[31] J. P. Perdew, K. Burke, M. Ernzerhof, Generalized gradient approximation made simple, Phys. Rev. Lett. 77 (18) (1996) 3865–3868.

[32] J. Tao, J. P. Perdew, V. N. Staroverov, G. E. Scuseria, Climbing the density functional ladder: Nonempirical meta: Generalized gradient approximation designed for molecules and solids, Phys. Rev. Lett. 91 (14) (2003) 146401.

[33] A. Ruzsinszky, J. P. Perdew, G. I. Csonka, O. A. Vydrov, G. E. Scuseria, Spurious fractional charge on dissociated atoms: Pervasive and resilient self-interaction error of common density functionals, J. Chem. Phys. 125 (19) (2006) 194112.

[34] C. Lee, W. Yang, R. G. Parr, Development of the colle-salvetti correlation-energy formula into a functional of the electron density, Phys. Rev. B 37 (1988) 785–789.

[35] S. Grimme, Semiempirical hybrid density functional with perturbative second-order correlation, J. Chem. Phys. 124 (3) (2006) 034108.

[36] S. P. Ong, O. Andreussi, Y. Wu, N. Marzari, G. Ceder, Electrochemical windows of room-temperature ionic liquids from molecular dynamics and density functional theory calculations, Chem. Mater. 23 (11) (2011) 2979–2986.

[37] S. Pandian, S. G. Raju, K. S. Hariharan, S. M. Kolake, D.-H. Park, M.-J. Lee, Functionalized ionic liquids as electrolytes for lithium-ion batteries, J. Power Sources 286 (2015) 204 – 209.

[38] O. Borodin, Relation between heat of vaporization, ion transport, molar volume, and cation- anion binding energy for ionic liquids, J. Phys. Chem. B 113 (36) (2009) 12353–12357.

[39] O. Borodin, J. Vatamanu, G. Smith, Bulk and interfacial behavior of ionic liquids from molecular dynamics simulations, ECS. Trans. 33 (7) (2010) 583–599.

[40] U. L. Bernard, E. I. Izgorodina, D. R. MacFarlane, New insights into the relationship between ion-pair binding energy and thermodynamic and transport properties of ionic liquids, J. Phys. Chem. C 114 (48) (2010) 20472–20478.

[41] A. D. Becke, Density-functional exchange-energy approximation with correct asymptotic behavior, Phys. Rev. A 38 (6) (1988) 3098–3100.

[42] P. Mori-Sánchez, Q. Wu, W. Yang, Orbital-dependent correlation energy in density-functional theory based on a second-order perturbation approach: Success and failure, J. Chem. Phys. 123 (6) (2005) 062204.

[43] Y. Zhao, D. G. Truhlar, A new local density functional for main-group thermochemistry, transition metal bonding, thermochemical kinetics, and noncovalent interactions, J. Chem. Phys. 125 (19) (2006) 194101, 01426.

[44] R. M. Balabin, Communications: Intramolecular basis set superposition error as a measure of basis set incompleteness: Can one reach the basis set limit without extrapolation?, J. Chem. Phys. 132 (2010) 211103.

[45] S. Grimme, S. Ehrlich, L. Goerigk, Effect of the damping function in dispersion corrected density functional theory, J. Comput. Chem. 32 (7) (2011) 1456–1465.

[46] E. R. Johnson, A. D. Becke, A post-Hartree–Fock model of intermolecular interactions, J. Chem. Phys. 123 (2) (2005) 024101.

[47] E. R. Johnson, A. D. Becke, A post-hartree-fock model of intermolecular interactions: inclusion of higher-order corrections, J. Chem. Phys. 124 (17) (2006) 174104–174104.

[48] J. G. Brandenburg, J. E. Bates, J. Sun, J. P. Perdew, Benchmark tests of a strongly constrained semilocal functional with a long-range dispersion correction, Phys. Rev. B 94 (11) (2016) 115144.

[49] C. Riplinger, F. Neese, An efficient and near linear scaling pair natural orbital based local coupled cluster method, J. Chem. Phys. 138 (3) (2013) 034106.

[50] J. Friedrich, B. Fiedler, Accurate calculation of binding energies for molecular clusters – assessment of different models, Chem. Phys. 472 (2016) 72–80.

[51] J. Friedrich, Efficient calculation of accurate reaction Energies—Assessment of different models in electronic structure theory, J. Chem. Theory Comput. 11 (8) (2015) 3596–3609.

[52] R. M. Richard, M. S. Marshall, O. Dolgounitcheva, J. V. Ortiz, J.-L. Brédas, N. Marom, C. D. Sherrill, Accurate ionization potentials and electron affinities of acceptor molecules i. reference data at the CCSD(T) complete basis set limit, J. Chem. Theory Comput. 12 (2) (2016) 595–604.

[53] S. Grimme, Improved second-order Møller–Plesset perturbation theory by separate scaling of parallel- and antiparallel-spin pair correlation energies, J. Chem. Phys. 118 (20) (2003) 9095–9102.

[54] F. Neese, A. Hansen, D. G. Liakos, Efficient and accurate approximations to the local coupled cluster singles doubles method using a truncated pair natural orbital basis, J. Chem. Phys. 131 (6) (2009) 064103.

[55] D. G. Liakos, M. Sparta, M. K. Kesharwani, J. M. L. Martin, F. Neese, Exploring the accuracy limits of local pair natural orbital coupled-cluster theory, J. Chem. Theory Comput. 11 (4) (2015) 1525–1539.

[56] J. Friedrich, J. Hänchen, Incremental CCSD (t)(f12*)| MP2: a black box method to obtain highly accurate reaction energies, J. Chem. Theory Comput. 9 (12) (2013) 5381–5394.

[57] J. Rezác, K. E. Riley, P. Hobza, S66: A well-balanced database of benchmark interaction energies relevant to biomolecular structures, J. Chem. Theory Comput. 7 (8) (2011) 2427–2438.

[58] A. L. Jesus, M. T. Rosado, I. Reva, R. Fausto, M. E. S. Eusébio, J. Redinha, Structure of isolated 1, 4-butanediol: Combination of MP2 calculations, NBO analysis, and matrix-isolation infrared spectroscopy, J. Phys. Chem. A 112 (20) (2008) 4669–4678.

[59] U. R. Fogueri, S. Kozuch, A. Karton, J. M. Martin, The melatonin conformer space: benchmark and assessment of wave function and DFT methods for a paradigmatic biological and pharmacological molecule, J. Phys. Chem. A 117 (10) (2013) 2269–2277.

[60] D. G. Liakos, F. Neese, Improved correlation energy extrapolation schemes based on local pair natural orbital methods, J. Phys. Chem. A 116 (19) (2012) 4801–4816.

[61] K. A. Peterson, D. Figgen, E. Goll, H. Stoll, M. Dolg, Systematically convergent basis sets with relativistic pseudopotentials. II. small-core pseudopotentials and correlation consistent basis sets for the post-d group 16–18 elements, J. Chem. Phys. 119 (21) (2003) 11113–11123.

[62] F. Neese, The ORCA program system, Wiley Interdiscip. Rev. Comput. Mol. Sci. 2 (1) (2012) 73–78.

[63] A. Schäfer, H. Horn, R. Ahlrichs, Fully optimized contracted gaussian basis sets for atoms li to kr, J. Chem. Phys. 97 (4) (1992) 2571–2577.

[64] F. Weigend, R. Ahlrichs, Balanced basis sets of split valence, triple zeta valence and quadruple zeta valence quality for h to rn: design and assessment of accuracy, Phys. Chem. Chem. Phys. 7 (18) (2005) 3297–3305.

[65] V. Ivaništšev, K. Kirchner, K. Karu, I. Lage-Estebanez, M. V. Fedorov, NaRIBaS: A scripting framework for computational modelling of Nanomaterials and Room Temperature Ionic Liquids in Bulk and Slab, www.github.com/vladislavivanistsev/NaRIBaS, 2015.

[66] A. McLean, G. Chandler, Contracted gaussian basis sets for molecular calculations. i. second row atoms, z= 11–18, J. Chem. Phys. 72 (10) (1980) 5639–5648.

[67] R. Krishnan, J. S. Binkley, R. Seeger, J. A. Pople, Self-consistent molecular orbital methods. XX. a basis set for correlated wave functions, J. Chem. Phys. 72 (1) (1980) 650–654.

[68] S. Kazemiabnavi, Z. Zhang, K. Thornton, S. Banerjee, Electrochemical stability window of imidazolium-based ionic liquids as electrolytes for lithium batteries, J. Phys. Chem. B 120 (25) (2016) 5691–5702.

[69] V. Ivaništšev, S. O'Connor, M. V. Fedorov, Poly(a)morphic portrait of the electrical double layer in ionic liquids, Electrochem. Commun. 48 (2014) 61–64.

[70] M. Galinski, A. Lewandowski, I. Stepniak, Ionic liquids as electrolytes, Electrochim. Acta 51 (26) (2006) 5567–5580.

[71] M. L. Batista, J. A. Coutinho, J. R. Gomes, Prediction of ionic liquids properties through molecular dynamics simulations, Curr. Phys. Chem. 4 (2014) 151–172.

[72] S. Glasstone, K. J. Laidler, H. Eyring, The theory of rate processes: the kinetics of chemical reactions, viscosity, diffusion and electrochemical phenomena, McGraw-Hill Book Company, Incorporated, 1941.

[73] G. Han, Z. Fang, M. Chen, Modified eyring viscosity equation and calculation of activation energy based on the liquid quasi-lattice model, Sci. China Phys. Mech. Astron. 53 (10) (2010) 1853–1860.

[74] A. P. Abbott, Application of hole theory to the viscosity of ionic and molecular liquids, Chem. Phys. Chem. 5 (8) (2004) 1242–1246.

[75] K. Karu, A. Ruzanov, H. Ers, V. Ivaništšev, I. Lage-Estebanez, J. M. García de la Vega, Predictions of physicochemical properties of ionic liquids with DFT, Computation 4 (3) (2016) 25.

[76] K. Karu, H. Ers, M. Mišin, J. Sun, V. Ivaništšev, Data for the article "Performance of SCAN density functional method for a set of ionic liquids", https://github.com/vilab-tartu/SCAN/tree/v.04, 2017, DOI: 10.5281/zenodo.292628.

[77] J. P. Perdew, A. Zunger, Self-interaction correction to density-functional approximations for many-electron systems, Phys. Rev. B 23 (10) (1981) 5048–5079.

[78] I. Lage-Estebanez, A. Ruzanov, J. M. G. d. l. Vega, M. V. Fedorov, V. B. Ivaništšev, Self-interaction error in DFT-based modelling of ionic liquids, Phys. Chem. Chem. Phys. 18 (3) (2016) 2175–2182.

[79] I. Lage-Estebanez, L. del Olmo, R. López, J. M. García de la Vega, The role of errors related to DFT methods in calculations involving ion pairs of ionic liquids, J. Comput. Chem. 38 (8) (2017) 530–540.

[80] J. P. Perdew, A. Ruzsinszky, J. Sun, M. R. Pederson, Paradox of self-interaction correction: How can anything so right be so wrong?, in: Advances In Atomic, Molecular, and Optical Physics, Elsevier, 2015, pp. 1—14.

[81] H. Kurig, M. Vestli, K. Tõnurist, A. Jänes, E. Lust, Influence of room temperature ionic liquid anion chemical composition and electrical charge delocalization on the supercapacitor properties, J. Electrochem. Soc. 159 (7) (2012) A944–A951, 00027.

[82] T. Romann, E. Anderson, P. Pikma, H. Tamme, P. Möller, E. Lust, Reactions at graphene | tetracyanoborate ionic liquid interface – new safety mechanisms for supercapacitors and batteries, Electrochem. Commun. 74 (2017) 38–41.

[83] J. Scheers, J. Pitawala, F. Thebault, J.-K. Kim, J.-H. Ahn, A. Matic, P. Johansson, P. Jacobsson, Ionic liquids and oligomer electrolytes based on the b(CN)4- anion; ion association, physical and electrochemical properties, Phys. Chem. Chem. Phys. 13 (33) (2011) 14953.

[84] H. Yoon, G. H. Lane, Y. Shekibi, P. C. Howlett, M. Forsyth, A. S. Best, D. R. MacFarlane, Lithium electrochemistry and cycling behaviour of ionic liquids using cyano based anions, Energy Environ. Sci. 6 (3) (2013) 979–986.

[85] N. Sanchez-Ramirez, V. L. Martins, R. A. Ando, F. F. Camilo, S. M. Urahata, M. C. C. Ribeiro, R. M. Torresi, Physicochemical properties of three ionic liquids containing a tetracyanoborate anion and their lithium salt mixtures, J. Phys. Chem. B 118 (29) (2014) 8772–8781.

[86] S. Viboud, N. Papaiconomou, A. Cortesi, G. Chatel, M. Draye, D. Fontvieille, Correlating the structure and composition of ionic liquids with their toxicity on vibrio fischeri: A systematic study, J. Hazard. Mater. 215-216 (2012) 40–48.

[87] E. E. Zvereva, S. A. Katsyuba, P. J. Dyson, A simple physical model for the simultaneous rationalisation of melting points and heat capacities of ionic liquids, Phys. Chem. Chem. Phys.

[88] L. M. Varela, J. Carrete, M. García, J. R. Rodríguez, L. J. Gallego, M. Turmine, O. Cabeza, Pseudolattice theory of ionic liquids, in: A. Kokorin (Ed.), Ionic Liquids: Theory, properties, new approaches, InTech, Shanghai, 2011, pp. 347–366, 00002.

[89] E. I. Izgorodina, U. L. Bernard, P. M. Dean, J. M. Pringle, D. R. MacFarlane, The madelung constant of organic salts, Cryst. Growth Des. 9 (11) (2009) 4834–4839.

[90] J. R. Sangoro, C. Iacob, A. Serghei, C. Friedrich, F. Kremer, Universal scaling of charge transport in glass-forming ionic liquids, Phys. Chem. Chem. Phys. 11 (6) (2009) 913–916.

[91] Y. Zhang, E. J. Maginn, Direct correlation between ionic liquid transport properties and ion pair lifetimes: A molecular dynamics study, J. Phys. Chem. Lett. 6 (4) (2015) 700–705.

[92] Z. Ren, A. S. Ivanova, D. Couchot-Vore, S. Garrett-Roe, Ultrafast structure and dynamics in ionic liquids: 2D-IR spectroscopy probes the molecular origin of viscosity, J. Phys. Chem. Lett. 5 (9) (2014) 1541–1546.

[93] J. F. Kincaid, H. Eyring, A. E. Stearn, The theory of absolute reaction rates and its application to viscosity and diffusion in the liquid state., Chem. Rev. 28 (2) (1941) 301–365.

[94] E. Cohen, Fifty years of kinetic theory, Physica A 194 (1) (1993) 229–257.

[95] P. A. Madden, M. Wilson, Covalent effects in ionic liquids, J. Phys.: Condens. Matter 12 (8A) (2000) A95.

[96] S. Bi, T. M. Koller, M. H. Rausch, P. Wasserscheid, A. P. Fröba, Dynamic viscosity of tetracyanoborate-and tricyanomethanide-based ionic liquids by dynamic light scattering, Ind. Eng. Chem. Res. 54 (11) (2015) 3071–3081.

[97] J. Salgado, T. Regueira, L. Lugo, J. Vijande, J. Fernández, J. García, Density and viscosity of three (2,2,2-trifluoroethanol + 1-butyl-3-methylimidazolium) ionic liquid binary systems, J. Chem. Thermodyn. 70 (2014) 101–110.

[98] L. F. Zubeir, G. E. Romanos, W. M. A. Weggemans, B. Iliev, T. J. S. Schubert, M. C. Kroon, Solubility and diffusivity of CO2 in the ionic liquid 1-butyl-3-methylimidazolium tricyanomethanide within a large pressure range (0.01 MPa to 10 MPa), J. Chem. Eng. Data 60 (6) (2015) 1544–1562.

[99] R. G. Seoane, S. Corderí, E. Gómez, N. Calvar, E. J. González, E. A. Macedo, Á. Domínguez, Temperature dependence and structural influence on the thermophysical properties of eleven commercial ionic liquids, Ind. Eng. Chem. Res. 51 (5) (2012) 2492–2504.

[100] M. Larriba, P. Navarro, J. García, F. Rodríguez, Selective extraction of toluene from n-heptane using [emim][SCN] and [bmim][SCN] ionic liquids as solvents, J. Chem. Thermodyn. 79 (2014) 266–271.

[101] U. Domańska, M. Królikowska, K. Walczak, Density, viscosity and surface tension of binary mixtures of 1-butyl-1-methylpyrrolidinium tricyanomethanide with benzothiophene, J. Solution Chem. 43 (11) (2014) 1929–1946.

[102] E. J. González, B. González, E. A. Macedo, Thermophysical properties of the pure ionic liquid 1-butyl-1-methylpyrrolidinium dicyanamide and its binary mixtures with alcohols, J. Chem. Eng. Data 58 (6) (2013) 1440–1448.

[103] U. Domańska, M. Królikowska, Density and viscosity of binary mixtures of thiocyanate ionic liquids + water as a function of temperature, J. Solution Chem. 41 (8) (2012) 1422–1445.

[104] M. Okuniewski, K. Paduszyński, U. Domańska, Effect of cation structure in trifluoromethanesulfonate-based ionic liquids: density, viscosity, and aqueous biphasic systems involving carbohydrates as "salting-out" agents, J. Chem. Eng. Data 61 (3) (2016) 1296–1304.

[105] H. Tokuda, S. Tsuzuki, M. A. B. H. Susan, K. Hayamizu, M. Watanabe, How ionic are room-temperature ionic liquids? an indicator of the physicochemical properties, J. Phys. Chem. B 110 (39) (2006) 19593–19600.

[106] I. Bandrés, F. M. Royo, I. Gascón, M. Castro, C. Lafuente, Anion influence on thermophysical properties of ionic liquids: 1-butylpyridinium tetrafluoroborate and 1-butylpyridinium triflate, J. Phys. Chem. B 114 (10) (2010) 3601–3607.

Appendices

On the Madelung constant

For the interpretation of the diffusional behavior of ionic liquids, the Bahe–Varela pseudolattice formalism proves to be useful [88]. Because of the long-range nature of ionic interactions, the longer-range order, ., pseudolattice, is expected in ionic liquids than in other types of electrolyte solutions. Among some assumptions of this simple model approach, we will highlight that the energy calculation errors, stemming from the approximation of a liquid by an ordered lattice, are expected effectively canceled. Therefore, the free energy difference coming from strong Coulomb and van der Waals interactions can be approximated:

$$\Delta G_{\text{ion}} = -\frac{M_{\text{Coulomb}}}{r} - \frac{M_{\text{vdW}}}{r^6}, \tag{5.1}$$

where M_{Coulomb} and M_{vdW} are multiplications of Madelung-like constants for Coulomb ($E \propto r^{-1}$) and van der Waals ($E \propto r^{-6}$) interactions, respectively, by a number of specific physical variables and constants which are omitted to retain clarity; r is the pseudolattice constant. The Madelung constant relates the structural features of a crystal with the interaction energy of the neighboring ions in the unit cells to give the corresponding lattice energy. As was shown by Izgorodina *et al.* it can be also applied to organic salts [89]. Within the pseudolattice formalism, we use the Madelung-like constants to define the free energy difference for an ion in both stable and transition states (Equation 5.1), when jumping from one cage to another (illustrated in Figure 4.6). The rate of the successful jumps (ω) over the rate-limiting energy barriers ($E^{\#}$) can be quantified:

$$\omega = \frac{k_B T}{h} P \exp\left(-E^{\#}/RT\right), \tag{5.2}$$

where k_B is the Boltzmann's constant, h is the Planck's constant, P is the probability of a cavity formation with a radius larger than $r/2$, and r is the jump-length proportional to the anion–cation distance. Note, for the self-diffusion coefficient (D) applies: $D \sim \omega/r^2$. Experimentally it was confirmed that ω is proportional to the conductivity (σ) for a set of 14 ionic liquids [90]. In simulations of 29 ionic liquids it was shown that the ion pair lifetime ($t \sim \omega^{-1}$) is inversely proportional to the conductivity [91]. As shown in the next section, through the Stokes–Einstein and Nernst–Einstein equations the conductivity is related to the diffusion coefficient and viscosity of an ionic liquid as $\sigma \sim D$ and $\sigma \sim \eta^{-1}$, respectively. Therefore, the interaction between the cation and anion plays a significant role in controlling the ion dynamics in ionic liquids. We suggest that the activation energy can be expressed as the difference between Madelung-like constants (ΔM) for ion in a stable and transition states. Consequently, under the approximations described above, the interaction energy of an ionic pair is theoretically related to the activation energy and the probability for the ion jump between two pseudolattice cages. The elegance of such approach is that ΔM serves as proportionality coefficient in Equation 3.16, and is

roughly the same for the investigated set of data. Moreover, taking into account that during the vaporization an ionic pair evaporates from the ionic liquid surface, the heat of vaporization can be approximated as: $\Delta H_{\text{vap}} \approx (M-1)E_{\text{int}}$. The latter expression provides an explanation to a number of derived D vs. ΔH_{vap} relations, discussed in Refs [38–40, 40].

The relation between viscosity and diffusion coefficient

In this work, we operate with viscosities instead of the diffusion coefficients, because there are more experimental data on the former. Ren *et al.* investigated ionic liquids with ultrafast two-dimensional IR spectroscopy [92]. Their results suggested that breaking up of the local ion-cage is the key event for activating translational diffusion and hence viscosity in ionic liquids. More generally, in substance with no chemical or electrical gradients (*i.e.*, pure ionic liquid at potential of zero charge) the viscosity (η) is inversely proportional to the self-diffusion coefficient (D):

$$\eta = \frac{k_B T \lambda_1}{\lambda_2 \lambda_3 D}, \tag{5.3}$$

where λ_1 and λ_2 are the pseudo-lattice constants in the plane parallel to where the observed diffusional movement takes place and λ_3 is the pseudo-lattice constant normal to the diffusional plane [93], k_B is the Boltzmann constant, and T is absolute temperature. When describing classical electrolyte solutions, the mobile charge carrier is related to its diffusion coefficient (D) through the Nernst–Einstein equation:

$$\Lambda = \frac{z^2 e^2 N_{\text{A}} D}{k_B T}, \tag{5.4}$$

where, z is the valence of the charge carrier, e corresponds to the elementary charge, N_{A} is the Avogadro's number. Also, the diffusion coefficient of a model spherical species of an effective radius r is inversely proportional to the medium viscosity, according to the Stokes–Einstein equation:

$$D = \frac{k_B T}{6\pi r \eta}. \tag{5.5}$$

The Nernst–Einstein relation was derived for non-interacting ions, such as in an infinitely dilute electrolyte solution. In real ionic liquids mass, momentum, charge, and energy transport processes which involve correlated collisions, caging, and vortex motions can also be taken into account [94]. In fragile ionic liquids where the structure is dominated by packing effects, the structural relaxation, which determines the transport properties, is that of the cage around each particle [95]. Nevertheless, from Equations 5.4 and 5.5 the following equation can be derived when taking into account that $N = nN_{\text{A}}$ and $\sigma = \Lambda n \div V$:

$$\Lambda = \frac{z^2 e_0^2}{6V\pi r} \frac{N}{\sigma}. \tag{5.6}$$

Therefore, the conductivity (σ) of a classical electrolyte solution is inversely proportional to the medium viscosity. The same applies to the ionic liquids, thus can be used in high-throughput calculations to evaluate conductivity values from the estimated viscosity values.

The experimental viscosity references

Ionic pair	T range (K)	η 298K (Pa · s)	η^{est} (Pa · s)
[BMIm][$B(CN)_4$]	283.40 – 351.99	0.069 [96]	0.0234
[BMIm][BF_4]	278.15 – 338.15	0.106 [97]	0.2751
[BMIm][$C(CN)_3$]	298.15 – 363.15	0.02784 [98]	0.0172
[BMIm][$N(CN)_2$]	293.15 – 343.15	0.03005 [99]	0.0509
[BMIm][SCN]	313.15 – 353.15	0.0322 (313K) [100]	0.0803
[BMIm][PF_6]	288.15 – 373.15	0.274 [97]	0.1620
[BMIm][TFMS]	293.15 – 343.15	0.0897 [99]	0.3763
[BMIm][TFSI]	278.15 – 373.15	0.0516 [97]	0.1210
[BMPyr][$C(CN)_3$]	308.15 – 358.15	0.0206 [101]	0.0100
[BMPyr][$N(CN)_2$]	293.15 – 343.15	0.0346 [102]	0.0327
[BMPyr][SCN]	298.15 – 348.15	0.109 [103]	0.0456
[BMPyr][TFMS]	293.15 – 363.15	0.164 [104]	0.2284
[BMPyr][TFSI]	283.15 – 353.15	0.0749 [105]	0.0604
[BPy][BF_4]	298.15 – 343.15	0.145 [106]	0.1437
[BPy][TFMS]	298.15 – 338.15	0.127 [106]	0.1318
[BPy][TFSI]	303.15 – 328.15	0.04915 (303K) [106]	0.0844

Table 5.1: The range of temperatures (T) of the fitted experimental viscosities, experimental viscosities (η) at 298 K, and the estimated viscosities (η^{est}).

DLPNO-CCSD(T) results

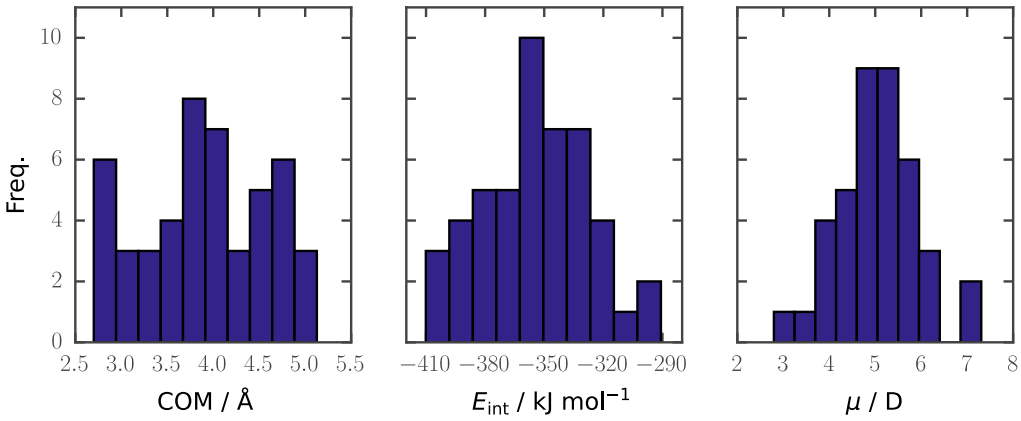

Figure 5.1: The distributions of distances between the geometric centers of cation and anion (left), cation and anion interaction energies (center), and dipole moments (right). The geometry of the pairs was obtained using the B2PLYP method and interaction energies and dipole moments are taken from DLPNO-CCSD(T) calculations.

	COM (Å)	E_{int} (kJ/mol)	μ (Debye)
[BMIm][$B(CN)_4$]	3.740	−312.506	6.008
[BMIm][BF_4]	3.268	−375.182	4.640
[BMIm]Br	2.891	−395.738	3.746
[BMIm][$C(CN)_3$]	2.980	−337.239	4.723
[BMIm]Cl	2.701	−408.563	3.386
[BMIm][FSI]	3.333	−354.762	4.342
[BMIm]I	3.043	−374.361	3.939
[BMIm][$N(CN)_2$]	2.718	−366.636	3.841
[BMIm][PF_6]	3.392	−355.486	4.981
[BMIm][SCN]	2.929	−379.105	4.107
[BMIm][TFMS]	3.901	−370.449	4.331
[BMIm][TFSI]	3.609	−351.285	4.330
[BMPyr][$B(CN)_4$]	4.457	−298.408	7.046
[BMPyr][BF_4]	3.873	−361.537	5.432
[BMPyr]Br	4.755	−386.698	5.231
[BMPyr][$C(CN)_3$]	3.740	−321.222	5.859
[BMPyr]Cl	4.565	−400.431	4.837
[BMPyr][FSI]	3.968	−338.548	5.566
[BMPyr]I	4.942	−359.732	5.596
[BMPyr][$N(CN)_2$]	3.462	−354.141	4.859
[BMPyr][PF_6]	4.248	−336.801	6.235
[BMPyr][SCN]	3.521	−363.222	5.056
[BMPyr][TFMS]	4.675	−358.533	5.127
[BMPyr][TFSI]	4.800	−331.784	5.393
[BPy][$B(CN)_4$]	4.693	−315.280	5.632
[BPy][BF_4]	4.005	−362.608	4.726
[BPy]Br	3.083	−388.812	3.493
[BPy][$C(CN)_3$]	4.055	−337.470	4.381
[BPy]Cl	2.928	−410.101	2.796
[BPy][FSI]	4.326	−343.253	4.393
[BPy]I	3.530	−379.889	3.388
[BPy][$N(CN)_2$]	3.708	−359.228	4.073
[BPy][PF_6]	4.452	−341.103	5.412
[BPy][SCN]	2.740	−369.828	3.973
[BPy][TFMS]	4.045	−348.481	4.628
[BPy][TFSI]	4.709	−340.659	4.752
[TEPA][$B(CN)_4$]	4.790	−290.772	7.306
[TEPA][BF_4]	3.963	−346.857	5.837
[TEPA]Br	4.231	−377.996	5.125
[TEPA][$C(CN)_3$]	3.794	−317.788	5.408
[TEPA]Cl	4.036	−391.353	4.728
[TEPA][FSI]	4.110	−333.423	5.252
[TEPA]I	4.428	−352.217	5.491
[TEPA][$N(CN)_2$]	3.779	−336.935	5.451
[TEPA][PF_6]	4.468	−331.974	6.309
[TEPA][SCN]	3.776	−357.415	5.165
[TEPA][TFMS]	4.933	−338.791	5.690
[TEPA][TFSI]	5.127	−321.754	5.733

Table 5.2: Distances between cation and anion center of masses (COM), their interaction energy computed with the reference method (E_{ref}) and the dipole moment of the ion pair (μ).

SCAN plot with specified ions

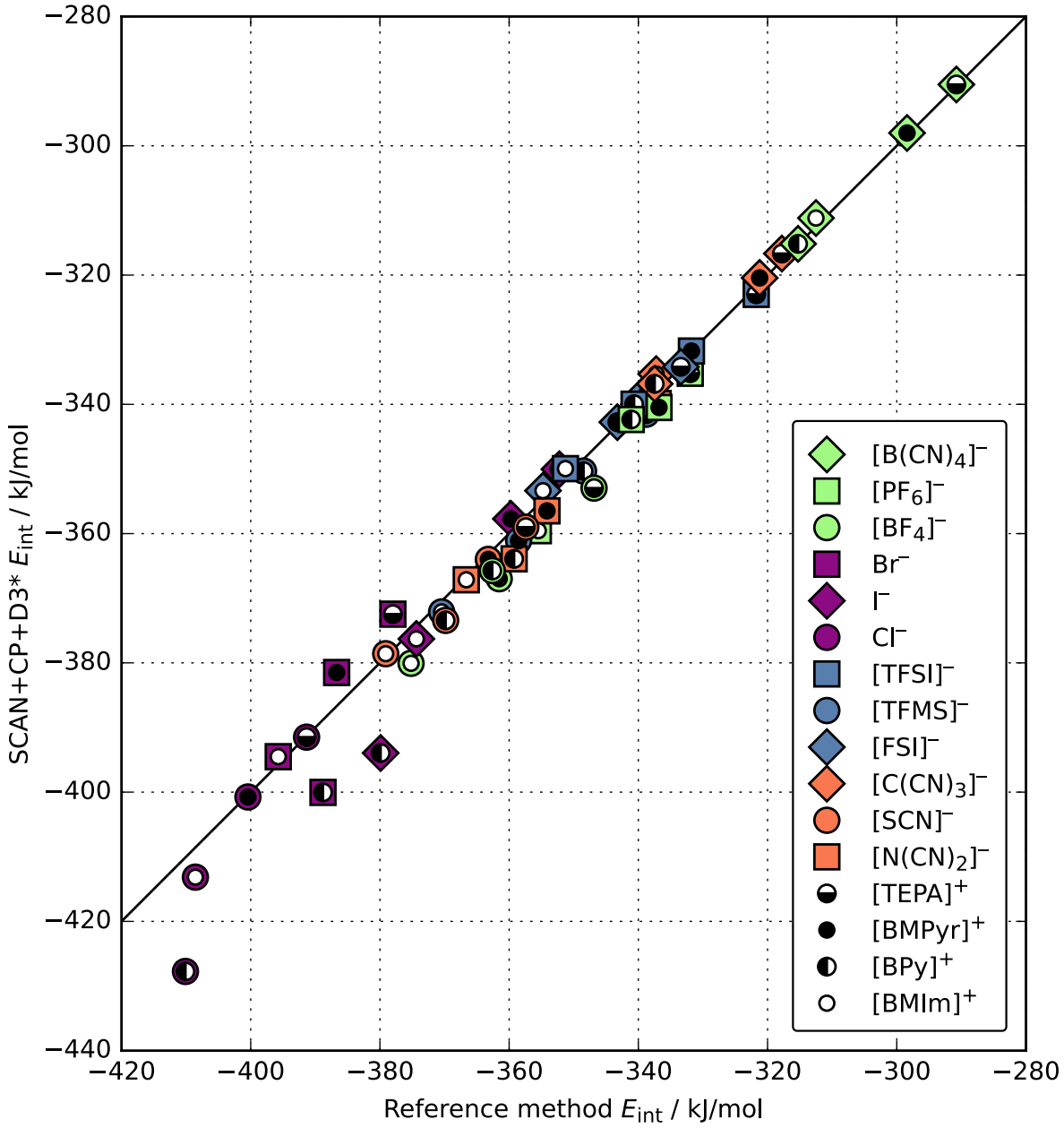

Figure 5.2: The performance of the corrected SCAN (with D3* and CP) versus the reference method. This Figure is similar to Figure 4.3 in the main article but contains additional information about the ionic pairs.

Non-exclusive license to reproduce thesis and make thesis public

I,

Karl Karu

(date of birth: 16.03.1993),

1. herewith grant the University of Tartu a free permit (non-exclusive license) to:
   (a) reproduce, for the purpose of preservation and making available to the public, including for addition to the DSpace digital archives until expiry of the term of validity of the copyright, and
   (b) make available to the public via the web environment of the University of Tartu, including via the DSpace digital archives from 18.05.2019 until expiry of the term of validity of the copyright,

   "Computational investigation of ionic liquids",

   supervised by Vladislav Ivaništšev ja Meeri Lembinen.
2. I am aware of the fact that the author retains these rights.
3. I certify that granting the non-exclusive license does not infringe the intellectual property rights or rights arising from the Personal Data Protection Act.

Tartu, **18.05.2017**